RSC Advances

REVIEW

View Article Online
View Journal | View Issue

Cite this: *RSC Adv.*, 2026, **16**, 30093

Insights into 3D-printed TiO_2-based architectures for photocatalytic and non-catalytic applications

Vaskuri C. S. Theja,†[a] Vaithinathan Karthikeyan, †[ab] Yifan Guo,[a] Chi Shun Yeung,[a] Sushantika Choudhary, [a] Venkatramanan Kannan, [c] Dani S. Assi, [ab] Gopalan Saianand, [d] Dong-Eun Lee,[ef] Gopalan Anantha Iyengar *[e] and Vellaisamy A. L. Roy*[ab]

Received 25th February 2026
Accepted 22nd May 2026

DOI: 10.1039/d6ra01640e

rsc.li/rsc-advances

3D printing has fundamentally transformed the design and engineering of photocatalytic materials, enabling the fabrication of geometrically complex, hierarchically structured TiO_2 to overcome the critical limitations of conventional approaches. This comprehensive review highlights advancements in the 3D printing of TiO_2, with a particular emphasis on fabrication methodologies, photocatalytic activity, performance optimization strategies, and other non-catalytic functional applications. The discussion encompasses the benefits of 3D-printed TiO_2 structures, including the fabrication of complex geometries and the optimization and enhancement of material performance, while also critically addressing the persistent challenges of scalability and operational stability. Recent advancements, including the incorporation of secondary dopants, the formation of synergistic composite materials, and surface modification strategies, are evaluated for their contributions to enhanced photocatalytic efficiency. Beyond photocatalysis, we also explore multi-functional applications in optical sensors, thermal-mechanical composites, and dental-orthopedic biomaterials, highlighting TiO_2's versatility across diverse technological domains. The unique capabilities of additive manufacturing facilitate the rational design of TiO_2 with tailored geometries and compositional complexity, positioning it as a promising platform for both laboratory-scale mechanistic studies and practical real-world remediation applications.

1. Introduction

Accelerated industrialization and rapid urbanization have led to widespread environmental degradation, primarily due to the accumulation of complex pollutants in aqueous and atmospheric systems. Among the most concerning consequences of this growth is the release of a complex array of pollutants, including heavy metals, nitrogen and sulfur compounds, and persistent organic contaminants, which severely compromise ecosystem strength and pose substantial risks to human well-being. The development of efficient, sustainable, and economically viable pollutant remediation technologies capable of mineralizing or sequestering such contaminants remains a demanding task for contemporary environmental engineering groups. Among the various remediation approaches, photocatalysis has emerged as a highly promising strategy, with TiO_2 being one of the most extensively studied and practically viable photocatalysts.[1] TiO_2 exhibits exceptional responsiveness to UV-visible light, robust charge carrier–photon interactions, high chemical and thermal stability, hydrophilicity, non-toxicity, and cost-effectiveness, which make it a highly attractive and affordable choice for environmental remediation.[2–4] TiO_2 is a semiconductor that generates reactive oxygen species (ROS), prominently hydroxyl ($^{\bullet}OH^{-}$), superoxide ($^{\bullet}O_2^{-}$) radicals, and electron–hole charge carriers under UV light irradiation, and is responsible for the photocatalytic degradation reactions.[3–5] In addition to its well-known photocatalytic properties, TiO_2 is also used for non-catalytic functional applications. Its optical properties, chemical inertness, and mechanical strength make it suitable for photonic devices, energy conversion systems, biomedical implants, and structural materials. These applications leverage TiO_2's multifunctional properties beyond catalysis, enhancing its versatility as a high-performance material across diverse technological domains.

[a]*School of Science and Technology, Hong Kong Metropolitan University, Ho Man Tin, Hong Kong. E-mail: vroy@hkmu.edu.hk*

[b]*Shenzhen Research Institute, Hong Kong Metropolitan University, Nanshan, Shenzhen, China*

[c]*Department of Physics, Sri Chandrasekharandra Saraswati Vishwa Mahavidyalaya, Enathur, Kanchipuram 631561, India*

[d]*Global Centre for Environmental Remediation, College of Engineering, Science and Environment, The University of Newcastle, Callaghan 2308, New South Wales, Australia*

[e]*Intelligent Construction Automation Centre, Kyungpook National University, Daegu 41566, South Korea. E-mail: algopal99@gmail.com*

[f]*School of Architecture, Civil, Environment and Energy, Kyungpook National University, 1370, Sangyeok-dong, Buk-gu, Daegu 702701, South Korea*

† Vaskuri C. S. Theja and Vaithinathan Karthikeyan contributed equally to this work.

In practice, one of the most significant challenges with TiO_2 (powder form) used in photocatalytic applications is maintaining its structural integrity, recovery, and reusability, as well as preventing cross-contamination (nanoparticle leaching). In conventional methods, such as dip coating and spraying, the photocatalytic rate is often low, leading to film damage from weak adhesion, non-uniform thickness, and excessive nanoparticle leaching. These limitations not only compromise the long-term efficiency and durability of the catalyst but also pose difficulties for safe recovery and recycling, thereby increasing the risk of environmental contamination and undermining the overall process's reliability. To overcome these problems, 3D printing technology offers a fresh, robust solution by enabling the production of structures with complex geometries tailored to specific environments, thereby improving structural, functional, and recovery–reuse properties.[6–8] 3D printing methods, including stereolithography (SLA), digital light processing (DLP), direct ink writing (DIW), fused deposition modelling (FDM), and fused filament fabrication (FFF), coating on the selective laser melting (SLM) or selective laser sintering (SLS), have transformed the fabrication of TiO_2 architectures, allowing the fabrication of intricate complex structures with high precision and customization. These technologies facilitate the integration of TiO_2 into polymeric composite matrices, enabling the development of hierarchically structured materials with improved photocatalytic activity. Their controlled, layer-by-layer deposition empowers the creation of gradient and spatially varied compositions, resulting in multifunctional materials that combine superior photocatalytic performance with enhanced mechanical properties. Moreover, the inherent versatility of 3D printing reduces material waste, increases design flexibility, and accelerates both prototyping and implementation. Given these distinctive capabilities, 3D printing is increasingly regarded as a viable and versatile platform for fabricating advanced photocatalytic reactors.[4,5] In addition, it is also considered a viable approach for building integrable photocatalytic reactor designs.[9,10] As statistically demonstrated in Fig. 1(a), research towards 3D-printed TiO_2 structures started in 2014–2015 and has rapidly progressed over the past few years. Nearly two-thirds of the research published on 3D-printed TiO_2 focused on photocatalytic applications.

By precisely adjusting the geometry and material composition, these 3D printing approaches significantly enhance photocatalytic efficiency and broaden the potential utility of TiO_2 across other domains. Fig. 1(b)–(d) display pie charts summarizing statistical research trends on 3D-printed TiO_2 for various applications. 3D-printed TiO_2 architectures are primarily used for photocatalytic wastewater treatment, antimicrobial and self-cleaning surfaces, air purification, H_2 production, and other photocatalytic and non-photocatalytic functional applications (as shown in Fig. 2).[11] In this review, we comprehensively described how 3D-printed TiO_2 serves as a multifunctional platform (wastewater treatment, antimicrobial surfaces, hydrogen production, air purification, N_2 fixation, optical/photonic, construction, thermal-mechanical, and biomedical applications), whereas the only existing earlier review was limited to organic pollutant degradation.[12] In this review, we discussed the details on various 3D printing methods and their performance (photocatalytic and non-catalytic) comprehensively, with dedicated subsections for methods, mechanisms, each application area, and a forward-looking summary.

2. 3D printing methods for TiO_2

3D printing is commonly used to fabricate membranes, monoliths, scaffolds, and filters for photocatalytic and other functional applications. 3D printing of TiO_2 encompasses various techniques, as per various studies, primarily grouped into four sections based on the printing mechanisms: DLP/SLA; DIW; FDM/FFF; and SLM/SLS, as shown in Fig. 3. Vat photopolymerization (DLP/SLA) relies on spatially resolved curing of a TiO_2-loaded photocurable resin in a liquid vat, using either a scanning laser (SLA) or projected digital light pattern (DLP) to solidify each layer. DLP/SLA method emerged as the leading choice for TiO_2 3D printing, because it offers sub-tens-of-micrometer resolution, high dimensional accuracy, and the ability to realize complex, thin-walled lattice architectures with high surface-to-volume ratio, which are advantageous for photocatalytic reactors and other functional components. Additionally, it enables the simple fabrication of TiO_2-based thin films on substrates for various applications.[13] Material extrusion covers both DIW and FDM/FFF, but the underlying working principles differ in the way the feedstock is delivered and solidified. DIW is an extrusion-based 3D printing method in which a viscous ink is pushed through a nozzle under pressure and deposited layer by layer to build the desired geometry. It is particularly suited to ceramic- or nanoparticle-rich inks, such as TiO_2 slurries, because their paste-like nature allows high solid loading while remaining printable. Shape retention is governed by ink rheology and rapid gelation or solvent loss after deposition, which makes DIW well-suited for open woodpile, honeycomb, and foam-like TiO_2 monoliths with hierarchical porosity. Unusually, Sopha *et al.* first DIW-printed the Ti woodpile and then anodized it to produce TiO_2 nanotubes on its surface.[14,15] FDM/FFF is a filament-based extrusion process in which a thermoplastic wire is heated, extruded through a nozzle, and deposited layer by layer. When TiO_2 is incorporated into the filament, this method enables low-cost, desktop fabrication of TiO_2-containing structures and scaffolds. FDM and FFF printing methods are also the same, except for their usage terminology (FDM is an industrial-grade method, while FFF is a desktop 3D printing method). Due to nozzle-based printing and low-layer resolution, both DIW and FDM/FFF are only used to fabricate monolithic woodpile scaffolds.[16]

Direct SLM/SLS 3D printing of TiO_2 is not widely adopted due to the difficulty of producing complex structures (primarily flat films), the significant effort required for powder handling and nitrogen environment, the high cost, and the high-power consumption.[17–20] Powder-bed-based SLM/SLS process, where a laser locally sinters or partially melts a powder layer to build the structures. In most cases, first SLM/SLS generates complex 3D metal scaffolds that are subsequently coated *via* anodization to form conformal TiO_2 nanotube layers, thereby combining the geometric freedom of powder bed fusion with the surface activity of TiO_2.[21–25] During coating to form a uniform,

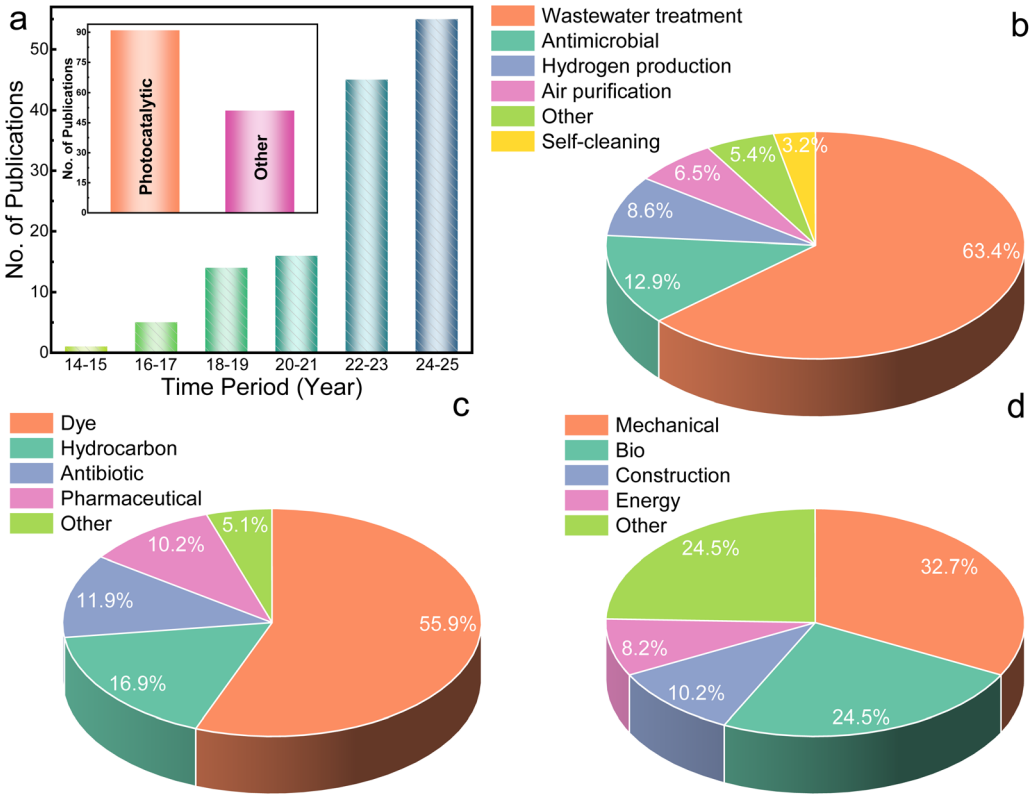

Fig. 1 Research statistical data from various studies of 3D-printed TiO_2 structures: (a) research articles published over the years, (b) photocatalytic applications, (c) photocatalytic degradations, and (d) other functional applications (filtered data in graphs is collected from the year 2014 to 2025 *via* Web of Science database using the keywords: TiO_2 and 3D-printing).

homogeneous TiO_2 coating on 3D structures, various parameters, such as electrolyte selection, heat-treatment time, and temperature, are critical.[24] Lastly, other 3D-printing methods, such as inkjet printing (IJP) and liquid deposition modeling, are also used to 3D-print simple thin-film TiO_2 structures for photocatalytic and solar cell applications.[26–28]

In addition, impregnating or dispersing secondary dopants (*e.g.*, metals or oxides) within the structures enhances photocatalytic or other functional activity. In most 3D printing methods, a significant amount of organic content is added: photoresin, photo initiator, binder, and/or dispersant in the DLP/SLA methods for light-based curing; PLA/ABS and binder in the FDM/FFF method for wire extrusion; and an organic solvent and binder in the DIW and IJP method for inkjet syringe flowability. Post-processing of printed structures, including heat treatments such as debinding, calcination, and/or pyrolysis/sintering, is necessary to eliminate or volatize most of the organic content. Step-wise controlled heat treatment is necessary to eliminate as much organic content as possible, without shrinkage or damage to the printed structures.[29] By controlling the process parameters, such as time, temperature, and environmental conditions of heat treatments, one can eliminate polymer degradation without compromising ceramic cracking, mechanical instability, phase instability, or structural collapse.[30] The overall advantages and limitations of the individual 3D printing methods are described clearly in Table 1. Compared with other methods, DLP/SLA offers the best solutions for producing TiO_2 parts with precise dimensional accuracy and complex, intricate application-oriented structures.

3. Photocatalytic performance and mechanistic considerations

Several investigations have demonstrated that the 3D-printed TiO_2 structures produced vigorous photocatalytic activity for various applications. The complete demonstration of 3D-printed TiO_2 structures (from their benefits and mechanisms to various photocatalytic applications) is shown in Fig. 4. The capacity of 3D printing to design bespoke geometries enables the creation of effective photocatalytic reactors and devices. The design freedom provided by 3D printing allows adjustment of flow dynamics and enhancement of the active surface area, thereby increasing the overall effectiveness of the photocatalytic process. After printing, the presence of TiO_2 on the surface of the structures is a critical factor regarding efficient photocatalytic reactions. As shown in Fig. 5(a), the common aligned and shifted geometric woodpile-type 3D-printed structures enhanced light penetration by a factor of 4 over the bulk structure on a macroscopic scale, strongly reflecting the high photocatalytic performance of 3D TiO_2 structures.[31]

In most studies, photocatalytic TiO_2 exists in two primary phases: rutile and anatase. The compound Degussa P25-TiO_2 consists of approximately 75% anatase and 25% rutile and is known for its high photocatalytic efficiency, making it the best

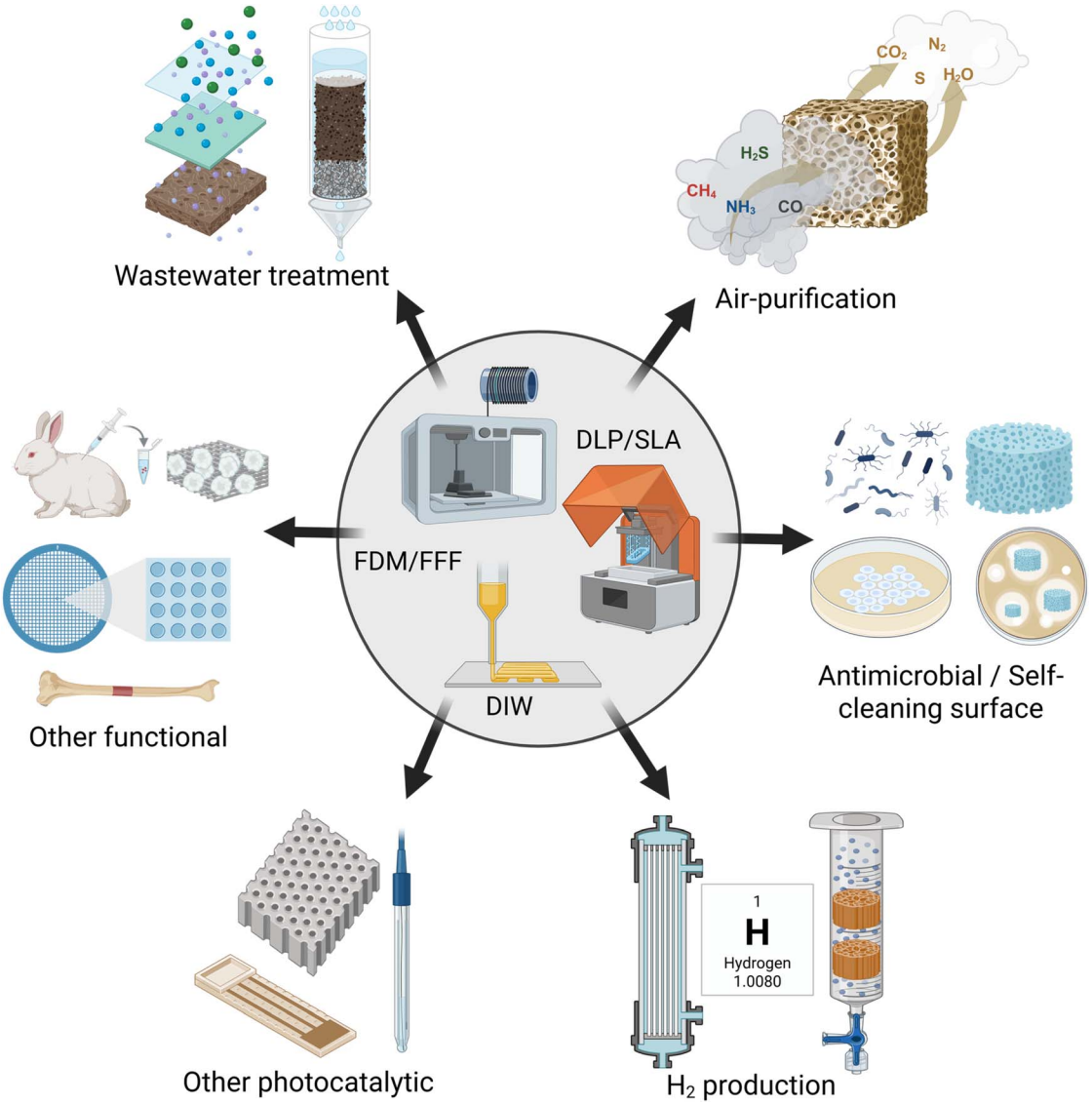

Fig. 2 Schematic demonstration of various applicable studies of 3D-printed TiO_2 structures and related primary printing methods.

choice to use in 3D-printed structures. As described in the previous section, heat treatment is critical for 3D-printed structures, as it primarily debinds and volatilizes the polymer content without transforming the TiO_2. For example, the volume of the 3D-printed TiO_2 structure compressed as the heat-treatment temperature increases, and the structure becomes more porous at high annealing temperatures, as shown in Fig. 5(b). For P25 TiO_2, the optimum heat treatment (180 °C for 30 min, then 250 °C for 30 min, then 350 °C for 30 min) applied to the printed structures does not alter the active anatase/rutile ratio.[32] In addition to post-treatment on the 3D-printing structures, the photocatalytic activity or other functionality is further enhanced by incorporating conductive elements, such as metals, graphene, oxides, or polyaniline, into TiO_2-printing structures. In photocatalysis, this boosts charge-carrier mobility and minimizes recombination rates by acting as co-catalysts or forming heterojunctions. The details of the 3D-printed structural designs, material optimizations, and related photocatalytic performances and other applications are explained in the following sections.

3.1 Wastewater treatment

The significant challenges in wastewater treatment or filtration systems are durable immobilization of catalyst materials, the high cost of catalytic filtration, and the potential for cross-contamination of treated water.[34] In addition, a large surface area and the hydrophilic nature of the catalyst material are required for the efficient photocatalytic degradation of pollutants; hence, balancing high surface area, hydrophilicity, durable immobilization, and cross-contamination is achieved by 3D printing of TiO_2. In addition, 3D-printed TiO_2 structures demonstrated strong reusability and recyclability in photocatalytic performance without compromising degradation efficiency.[35] A simple 3D-printed TiO_2-based lattice architecture enabled safe, strong, portable, self-supporting, efficient, and high-surface-area water disinfection without the need for

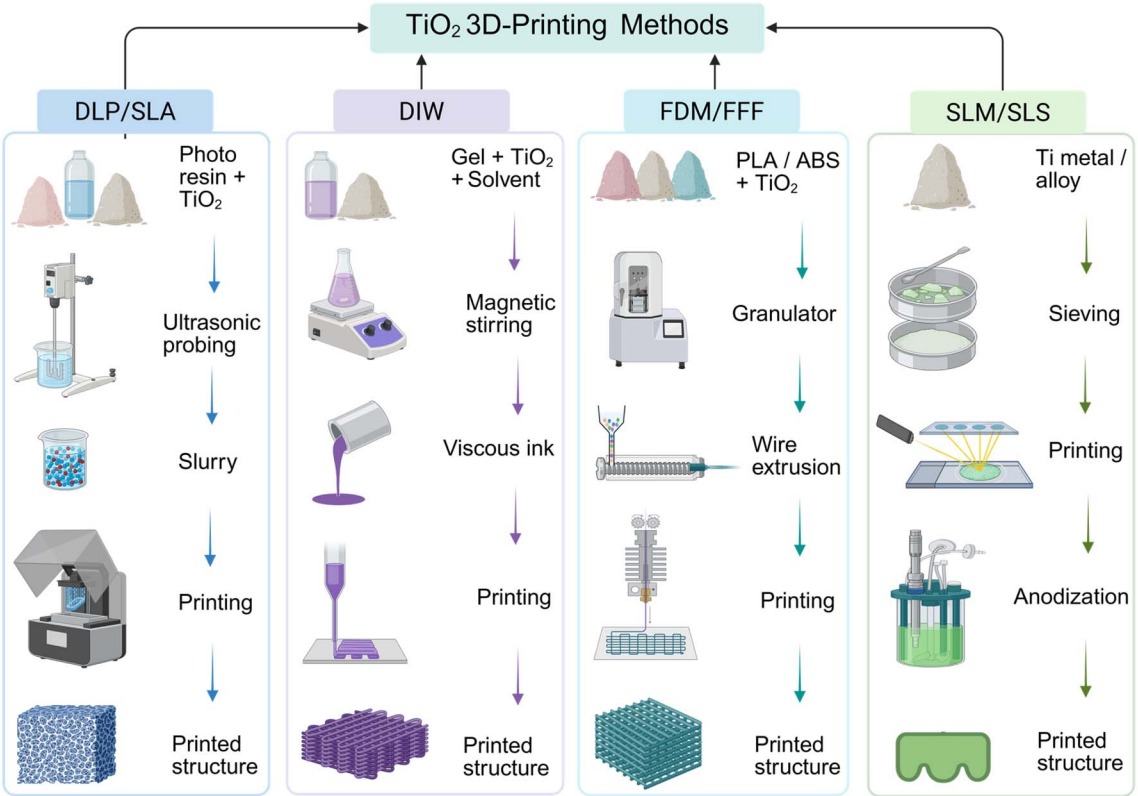

Fig. 3 Schematic demonstration of pronounced TiO_2 3D-printing routes (DLP/SLA, DIW, FDM/FFF, and SLM/SLS) and their standard fabrication processing steps and usual geometrical printed structures.

expensive, complex catalytic filtration.[34] The complete schematic demonstration (from material mixture to 3D printing to installation and UV exposure) of water purification using 3D-printed TiO_2 is shown in Fig. 6(a). Zhou *et al.* prototyped and designed a 3D-printed sinusoidal TiO_2-based photocatalytic flow reactor for wastewater purification.[36] The comparison of the degradation performance of 3D-printed TiO_2 architectures with conventional powder and thin-film materials is shown in Fig. 6(b). From the figure, it is clear that 3D-printed TiO_2 structures significantly improve the photocatalytic degradation performance compared with conventional powders and bulky structures.

Methylene blue (MB) is a well-studied organic dye for the photocatalytic degradation of organic pollutants using various 3D-printed TiO_2 structures. The degradation efficiency of various organic dyes reached over 90% using the optimal 3D-printed TiO_2 structure (Fig. 6(c)). As summarized in Table 2, the degradation rates and efficiencies varied significantly due to

Table 1 Advantages and limitations of various 3D-printed TiO_2 methods[12]

Method	Key advantages	Main limitations
DLP/SLA	• High-dimensional accuracy helps to produce complex, intricate structures • High printing resolution (sub-tens-of-micrometer) and faster printing rate • Enable complex, thin-walled structures with a high surface-to-volume ratio	• Additional post-treatments (curing, thermal treatments)
DIW	• Suited for high TiO_2 loading • Easier printability and cost-effective	• Only suitable for limited monolithic scaffold-type structures • Limited or poor lateral resolution and demanding rheological content
FFF/FDM	• Low-cost and widely accessible process • Produce robust, stable TiO_2 structures • Suitable for both lab-scale and industrial printing	• Very low layer resolution and low TiO_2 content • Restricted to simple scaffold designs • High polymer fraction
SLM/SLS	• Self-supporting metallic scaffold • Mechanically very strong	• High capital cost and energy-intensive • High wastage of the raw material and complex powder handling

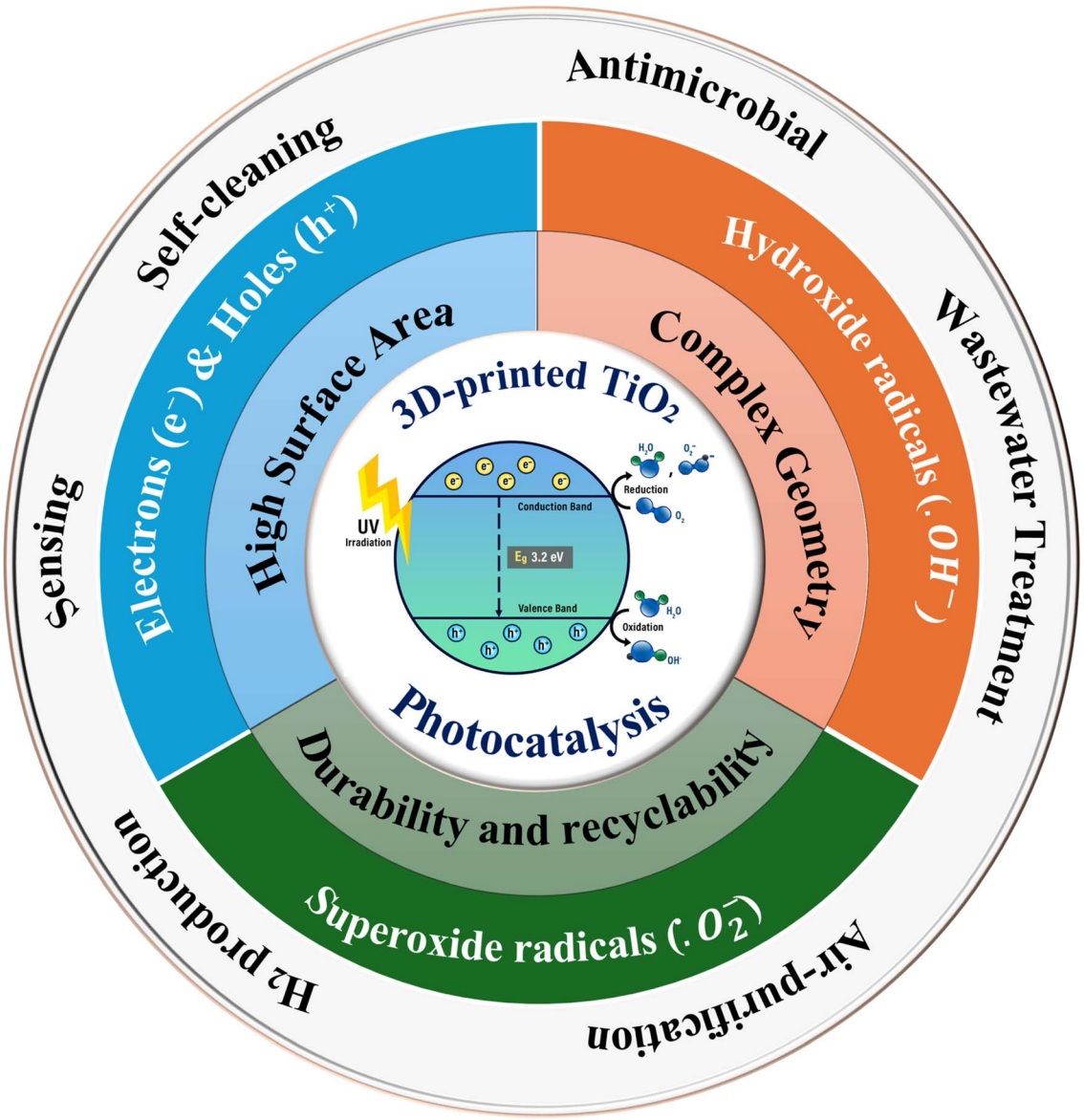

Fig. 4 Schematic illustration of the photocatalytic mechanism and possible reactive species generation, and additional benefits of 3D-printed TiO_2 across various photocatalytic applications.

the adopted 3D printing method, the TiO_2 loading concentration in the structures, and the additional loading of additives and dopants. Various optimization methods have been adopted to enhance the photocatalytic degradation performance. For example, the novel hierarchical 3D hollow microarchitecture, composed of a TiO_2/Fe_2O_3 heterojunction, facilitates the degradation of MB and acetaminophen *via* a solar-driven photo-Fenton catalytic reaction.[33] In another study, anodized TiO_2 nanotubes on 3D Ti–1% Nb meshes exhibited the highest acetaldehyde photocatalytic activity, owing to a reduced bandgap resulting from Nb defects introduced into the nanotubular crystalline lattice and minimal electron–hole recombination.[15] In another study, adding CNTs to a 3D structured compound parabolic reactor composed of TiO_2 improved photocatalysis and photolytic cleavage of amoxicillin pollutants.[69] Overall, incorporating secondary elements/compounds and optimizing structures with a high surface area and enhanced convective mass transport during 3D printing of TiO_2 results in enhanced photocatalytic wastewater treatment.

In addition to photocatalytic degradation of organic pollutants, 3D-printed TiO_2 structures are used in other wastewater treatment applications. For instance, a nanofiltration membrane made of DLP 3D printing with a TiO_2 and PEC-COOH active layer improves both hydrophilicity and permeation flux, while retaining 98.76% of the salt, demonstrating strong chlorine resistance and thus a high desalination capability for seawater.[83] Oil–water separation is crucial, particularly in offshore oil transportation, where frequent accidents harm the marine ecosystem and cause severe water pollution. In this regard, a 3D-printed composite membrane comprising an optimized ratio of TiO_2 and ABS efficiently rejects oil by promoting both hydrophilicity and oleophobicity.[84]

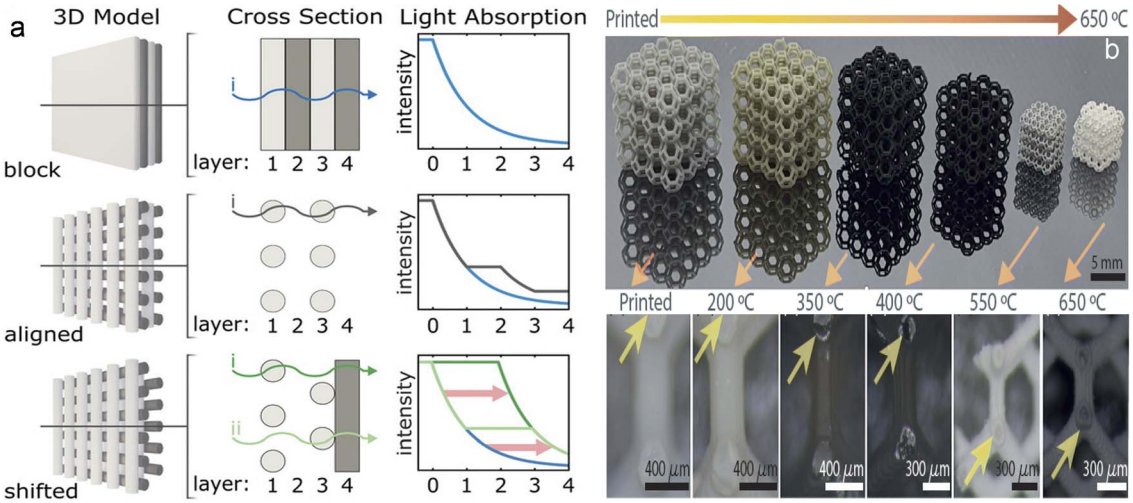

Fig. 5 (a) Schematic demonstration of the various structures, light penetration mechanism, and light absorption enhancement with the number of layers in the 3D-printed structures.[31] (b) 3D-printed TiO_2 structure and its volume compressed with increasing the heat treatment temperatures.[33]

3.2 Antimicrobial and self-cleaning surfaces

TiO_2 effectively damages or destroys microbes, primarily by generating reactive oxygen species (ROS), and induces DNA-cleaving oxidative reactions by damaging cellular membranes *via* UV irradiation. For example, FDM 3D-printed TiO_2 exhibits strong antibacterial performance, with 99.99% inhibition of *S. aureus* and 99.99% degradation of *E. coli*.[85] In another study, an SLS 3D-printed structure coated with TiO_2 exhibits antibacterial performance, achieving 90.11% and 90.60% degradation against *S. aureus* and *E. coli*, respectively.[25] As shown in Fig. 7(a), the 3D-printed TiO_2 pellets exhibited strong inhibition zones against *S. aureus* and *E. coli*, with inhibition zone diameters increasing with TiO_2 concentration.[86] In another antimicrobial study, *S. aureus* and *P. aeruginosa* are inhibited by TiO_2 agents incorporated into chitosan- or alginate-based macroporous 3D-printed hydrogels.[87,88] As shown in Fig. 7(b), the dispersion of Au nanoparticles on the 3D-printed Ti-structured TiO_2 anodized surface improved the antibacterial activity against *S. aureus* stained with acridine orange and ethidium bromide.[22] For the practical demonstration, 3D-printed and surface-coated TiO_2 strongly degraded *E. coli* in the 3D-printed water processor tank.[89] In another practicality, the 3D-printed TiO_2 and mulberry anthocyanins-based bacteriostatic chromogenic structure inhibited *S. aureus* and *E. coli*, thus improving the quality (shelf life and freshness) of litchi fruit.[90] In addition, the viruses, such as Human Coronavirus 229E and Feline Calicivirus, are inhibited by 70% and 60%, respectively, after 4 hours of exposure to the 3D-printed TiO_2 structural surface.[91]

3D printing technology can produce the required rough surfaces by optimizing layer thickness and incorporating hydrophobic and photocatalytic fillers into printed parts, thereby enhancing the self-cleaning ability of the geometries. For instance, Zhan *et al.* 3D-printed and designed a self-cleaning surface by incorporating TiO_2 and SiO_2 fillers into a polyurethane matrix, demonstrating improved hydrophobicity and roughness, as well as enhanced MB degradation.[17] As shown in Fig. 7(c), the addition of TiO_2 to the cement confers self-cleaning properties (color change upon exposure of the surface to RB dye) and improves the performance over time. Therefore, 3D-printed TiO_2 structures make systems and surfaces cleaner and safer.[92]

3.3 Hydrogen production

TiO_2 is a well-established photocatalyst for water splitting and the reduction of methane or ethane to produce H_2 gas. Compared to traditional powder, the 3D-printed TiO_2 monolith demonstrated higher H_2 production due to enhanced interaction between incident light and the printed catalyst, resulting from its higher surface area, hierarchical micro- and nanopores, and optimized size/shape.[93,94] For instance, as shown in Fig. 8(a), the design-optimized and hierarchically 3D-printed TiO_2 nanoporous aerogel with FCC lattice scaffolding demonstrated efficient light permeation and light harvesting, resulting in a hydrogen production rate almost five times higher than that of TiO_2 powder, which is further enhanced by dispersing Au nanoparticles.[95] Various design and engineering strategies are explored and adopted to improve the H_2 evolution rate with a 3D-TiO_2 structure. For instance, Schreck *et al.* designed a 3D polymer scaffold *via* DLP printing and then incorporated TiO_2/Pd aerogels into it.[96] In a comparative study, as shown in Fig. 8(b), with 3D-printed structural design optimization, he successfully demonstrated a 200% increase in hydrogen production rate, facilitated by greater UV light penetration and an enhanced reactive gas flow rate in the optimized structure.

The engineering strategy of pre- and post-impregnating Au nanoparticles into the TiO_2 3D-printed monoliths resulted in improved H_2 production from the water–ethanol mixture, especially in post-impregnation and calcination-treated monoliths.[99] In another case, TiO_2 is combined with a metal–organic framework, and the printed structure is then coated with Pt/PtO_x species, providing additional co-catalytic active sites and significantly enhancing the photocatalytic H_2 evolution

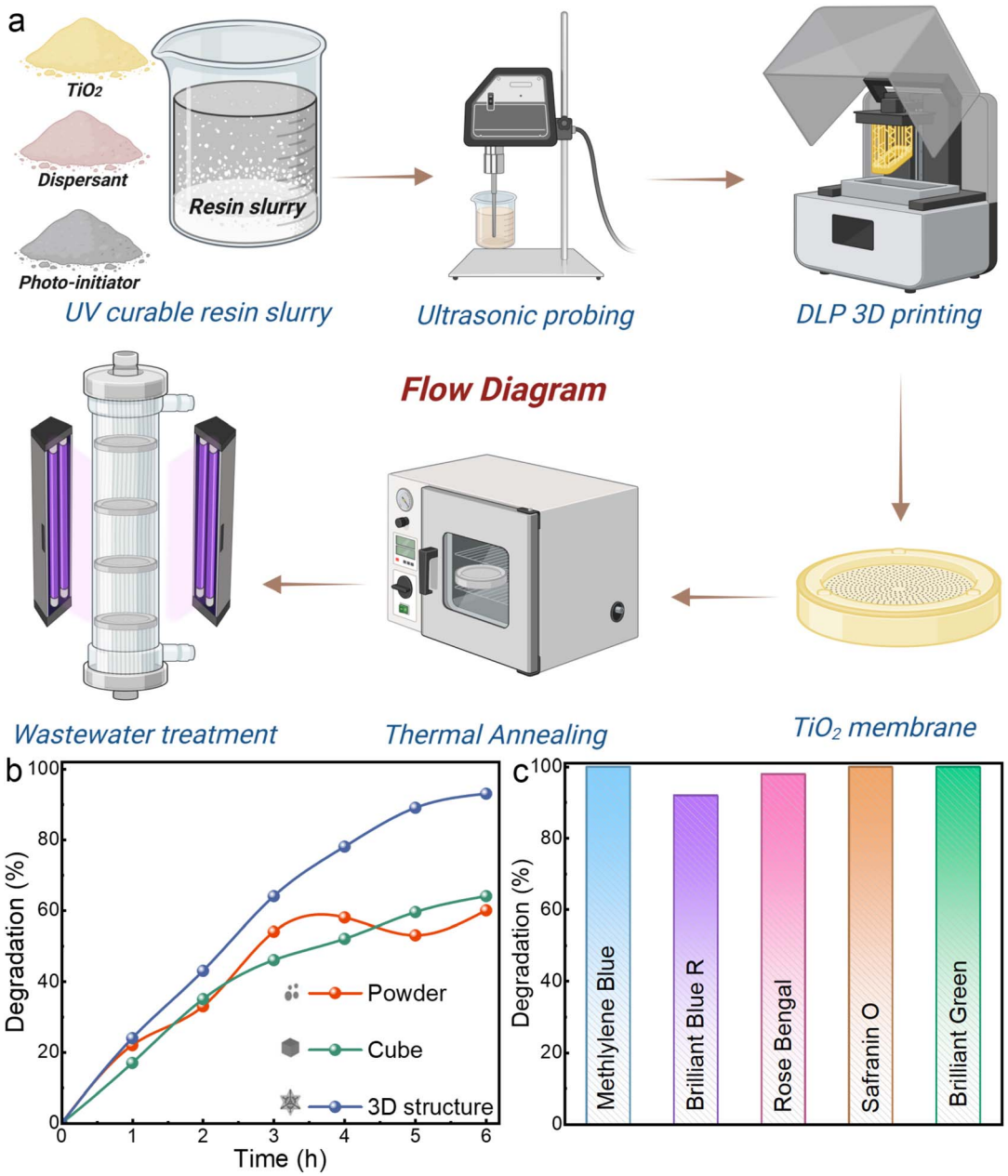

Fig. 6 (a) Schematic demonstration of the most-adopted 3D printing processing route towards wastewater treatment (from initial resin preparation to DLP 3D printing to post-processing to final photocatalytic activity of wastewater treatment). (b) Comparison of the methylene blue photocatalytic degradation performance of conventional TiO_2 powder and bulk cube with 3D-printed structure,[37] and (c) degradation efficiencies of various organic dyes with a 3D-printed TiO_2 structure. Reproduced with permission from American Chemical Society.[35] Copyright 2024.

reaction.[93] Furthermore, the designed and 3D-printed metal-based conical arrays of photoelectrodes are then anodized to form TiO_2 nanotubes, resulting in a significant enhancement in hydrogen production *via* photoelectrochemical water splitting.[21] Next, the recyclability and reusability of the 3D-printed TiO_2 for H_2 production are robust, as evidenced by a 0.5% reduction in H_2 production rate after 5 cycles (Fig. 8(c)).[93] In addition, PLA 3D-printed TiO_2/Au-coated microreactor demonstrated a strong long-term photocatalytic ability for two days (Fig. 8(d)), revealing a stable hydrogen photoproduction rate in a water–ethanol gas mixture.[97] Furthermore, the designed micro- and macroscopically porous 3D-printed structure, consisting of TiO_2 nanotube arrays and Pt nanoparticles, demonstrates excellent H_2 evolution reaction performance and long-term stability due to its unique porous architecture, high active surface area, strong electronic metal–support interactions, and efficient carrier transport.[98] Overall, as shown in Fig. 8(e), overpotential (η) comparison of various reported hydrogen evolution reaction electrocatalysts, the 3D-printed structure consisting of TiO_2 outperforms (should be low η for high H_2 production) the most advanced platinum-based catalysts.

Table 2 Summary of photocatalytic degradation performance of various 3D printed TiO_2-based systems

Material	Method	3D-structure	Load (%)	Pollutant	Degradation efficiency (%)	Irradiation time (h)	Rate constant (h^{-1})	Ref.
TiO_2	DLP	Diamond	50	Methylene blue	99	10	0.76	35
TiO_2	DLP	Octet	20	Methylene blue	93	6	—	37
TiO_2	DLP	Gyroid	36	Carbamazepine	40	2	—	38
TiO_2	DLP	Square grid	10	Rhodium B	85.8	6	0.28	39
TiO_2/CdS	DLP	NPR	9	Rhodium B	100	1.25	—	40
TiO_2/graphene	DLP	BCC	0.5	Methylene blue	82.9	5	0.34	41
TiO_2/Fe_2O_3	DLP	Kelvin	2	Methylene blue	95	3	—	33
TiO_2/Fe_2O_3	DLP	Kelvin	2	Acetaminophen	100	2	2.72	33
TiO_2	SLA	FCC	2	Arsenite	99.7	24	0.78	42
TiO_2	SLA	Cylindrical fan	1	Rhodium B	80	4	—	10
TiO_2/SiO_2	SLA	Hexagonal scaffold	5	Methylene blue	81.9	8	—	43
TiO_2/SiO_2/Sr	SLA	—	5	Methylene blue	84.5	8	—	44
TiO_2	DIW	Woodpile	—	Tetracycline	94.3	3.5	—	45
TiO_2	DIW	Woodpile	20	Methylene blue	100	1.25	—	46
TiO_2	DIW	Honeycomb	66.5	Rhodium B	99	3.2	1.14	47
TiO_2	DIW	Woodpile	63	Primidone	50	3	0.16	48
TiO_2	DIW	Film	10	Ciprofloxacin	46	4	0.30	49
TiO_2	DIW	Film	3	Methylene blue	84.6	2	0.40	50
TiO_2	DIW	Woodpile	63	Triclosan	99.5	4	0.66	51
TiO_2	DIW	Woodpile	4.1	Methylene blue	92	10	—	52
TiO_2	DIW	SLDD	2.2	Acesulfame	79	1	—	53
TiO_2	DIW	Hollow foam	—	Methylene blue	97	3.33	1.05	54
TiO_2	DIW	Woodpile	1	Amoxicillin	99.4	3	0.94	55
TiO_2/Pd	DIW	Woodpile	45	4-Nitrophenol	100	0.17	44.16	56
TiO_2/Pd	DIW	Pillars	—	4-Nitrophenol	99	0.33	16.2	57
TiO_2/Pd	DIW	Woodpile	20	4-Nitrophenol	100	0.25	—	58
TiO_2	IJP	Film	—	Rose Bengal	92	5	0.51	28
TiO_2	FDM	Film	40	Acetaminophen	74	0.66	1.68	59
TiO_2	FDM	Disk	20	Fluoranthene	91	24	0.1	60
TiO_2	FDM	Disk	20	Pyrene	94	24	0.12	60
TiO_2	FDM	Gyroid	20	Microcystin	95.5	8	0.37	61
TiO_2	FDM	F-RD	2.5	Methylene blue	93.4	2.5	—	62
TiO_2	FDM	Gyroid	10	Methylene blue	81.5	12	—	63
TiO_2	FDM	Square mesh	0.25	Methylene blue	13.5	2	—	64
TiO_2	FDM	Woodpile	30	Methyl orange	100	24	0.04	65
TiO_2	FDM	Dog-bone	10	Rhodium 6 G	22	4	—	66
TiO_2/Ag	FDM	Square mesh	1	Acetaminophen	98	2	1.98	67
TiO_2	FFF	Gyroid	37.5	Methyl orange	80	24	0.08	68
TiO_2	FFF	Helix	1.5	Amoxicillin	5.3	2	0.03	69
TiO_2	FFF	Diamond	34	Methylene blue	100	5	0.86	70
TiO_2	FFF	Diamond	34	Microcystin	100	24	0.24	70
TiO_2/AgCl/Ag	FFF	Gear	50	Methylene blue	99	1.7	2.25	71
TiO_2/Cu	3D coating	Gyroid	—	Tetracycline	93.6	1	2.4	72
TiO_2	3D coating	Woodpile	—	Methylene blue	91.8	0.8	3.0	14
TiO_2	3D coating	Hologram	—	Methylene blue	91	0.5	3.54	73
TiO_2	3D coating	BCC	5.4	Methylene blue	94.1	3	—	74
TiO_2	3D coating	Monolith	—	Rhodium B	62	20	—	75
TiO_2	3D coating	Octahedral	—	Methylene blue	92.5	3	—	76
TiO_2	3D coating	Thin film	—	Benzothiazole	98	2	1.96	77
TiO_2	3D coating	Thin film	—	Methylene blue	93	3.5	0.76	77
TiO_2/Ag	3D coating	Cylinders	—	Rhodium B	94.5	3	—	78
TiO_2/Ag	3D coating	Spiral	—	Rhodium B	30	5.83	0.07	79
TiO_2/SiO_2	3D coating	Rectangular mesh	—	Triton X-100	70	1.5	—	80
TiO_2/ZnO	3D coating	Tetrapod	—	Tetracycline	90	2.5	0.92	81
TiO_2/Cu/GO	3D coating	Gyroid	—	Methylene blue	93	2	—	82

3.4 Air purification

TiO_2 is also known for reducing CO_2 and other toxic gases, such as NO, NO_2, O_3, LPG, and CH_3CHO, through its photocatalytic ability. For CO_2 reduction, Chen *et al.* fabricated an artificial leaf structure with TiO_2 by direct ink writing, which artificial photosynthesis *via* photo-reduction (enhances CO and CH_4 evolution).[100] In another instance, the heterojunction of TiO_2 with $MoSe_2$, with an optimal infill percentage in the 3D-printed structure, resulted in a CO_2 selectivity of approximately 82% through enhanced visible-light absorption, delayed

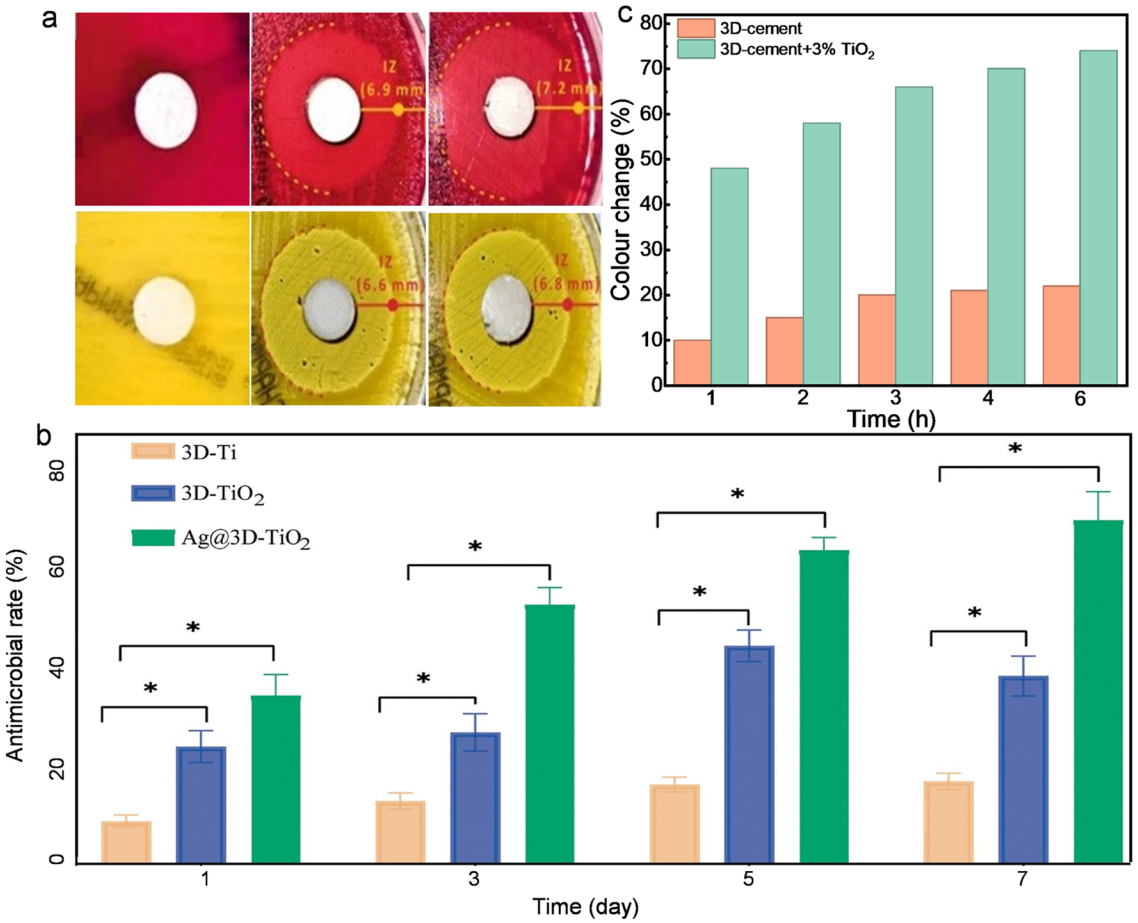

Fig. 7 (a) Antimicrobial susceptibility performance analysis on *E. coli* (red colonies) and *S. aureus* (yellow colonies) with increasing TiO_2 concentration (from left to right figures). Reproduced with permission from Springer Nature.[86] Copyright 2022. (b) Semi-quantitative graphs of antimicrobial activity of *S. aureus* on 1, 3, 5, and 7 days.[22] (c) Enhancing the self-cleaning ability of cement with the addition of a small amount of TiO_2.[92]

recombination of electron–hole pairs, and promoted charge transfer of photogenerated electrons.[101] Next, designed and fabricated a 3D-printed sinusoidal air-purifying photocatalytic reactor, made of a PLA and TiO_2 composite, which effectively removed 99% of O_3 and partially removed NO, NO_2, and CH_3CHO pollutants from the air.[102] Next, to examine the effect of TiO_2 morphology on the removal of NO_x (both NO and NO_2) as gaseous pollutants, the 3D-printed UV100-TiO_2 showed higher degradation efficiency than P25-TiO_2, although its selectivity was poorer.[103]

3.5 Other photocatalytic applications

Various other catalytic applications, such as N_2 photo-fixation, photoelectrochemical sensing, and photoanodes for batteries, are studied using 3D-printed TiO_2 structures. The designed macro- and micro-hierarchical, 3D-printed TiO_2 scaffold exhibits excellent potential for high surface adsorption and activation capacity, thereby promoting N_2 photo-fixation (the conversion of nitrogen to ammonia or other beneficial compounds).[11] In another instance, as shown in Fig. 9(a), novel designed 3D-printed hierarchical plasmonic heterostructure composed of vertical TiO_2 pillar arrays (as tree trunks), dense nanorod arrays (as branches), and plasmonic Au nanoparticles (as leaves) demonstrated a 15-fold high N_2 photo-fixation activity than its film due to the structure driven high active photocatalytic sites, multi-scattering of light, and enhanced plasmonic light absorption.[104] The 3D-printed TiO_2 hierarchical nanowire arrays with nanocavities have a greater surface area, more active sites, and shorter diffusion lengths for molecules during surface adsorption and reaction, thereby reducing response times and increasing sensitivity, resulting in an excellent photoelectrochemical sensor that surpasses a commercial P25-TiO_2 sensor.[105] In another study, a 3D-printed TiO_2/graphene/PANI-based molecularly imprinted micro-lattice-shaped photoelectrochemical sensor was developed, featuring a structure with designed, porous, interconnected macro-channels that enable the rapid spreading of incident light into the sensor interior, yielding high light absorption and highly efficient analyte diffusion/trapping throughout the entire sensor. The fabricated sensor demonstrated impressive ultra-sensitive urea monitoring, with rapid response, low detection limit, wide linear range, exceptional selectivity, and stable operation.[106] A 3D-printed photocathode made of an oxygen vacancy-rich, hierarchically porous rutile TiO_2/rGO/CNT

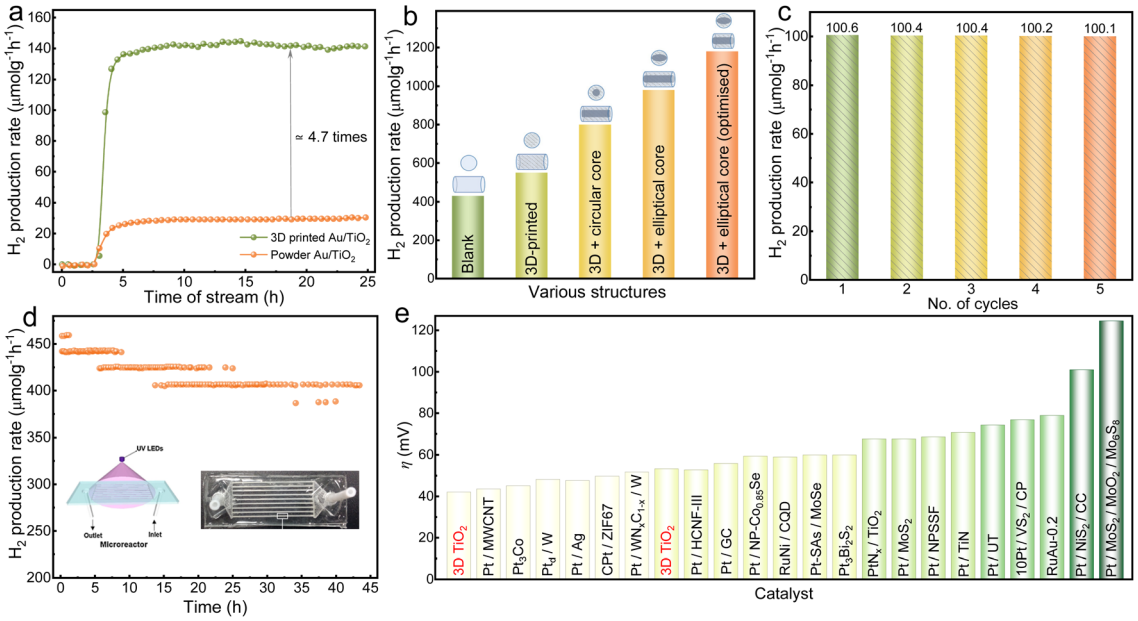

Fig. 8 (a) H_2 production rate of 3D-printed TiO_2 compared to conventional powder TiO_2.[95] (b) H_2 production rate enhancement with structural modifications on the 3D-printed structure.[96] (c) Strong recyclability of H_2 production with a TiO_2 3D-printed structure.[93] (d) Stable production of H_2 over long time in a designed 3D-printed TiO_2 microreactor.[97] (e) Comparison of the overpotential of 3D-printed TiO_2 structures (low overpotential indicates high H_2 production) with other reported H_2 production catalysts.[98]

structure delivers a high discharge current density with a stable, long-life cycle, attributed to efficient photocatalytic sites and fast electronic/ionic pathways for efficient battery applications.[107]

4. Other functional applications

Besides catalytic applications, 3D-printed TiO_2 structures are being explored in other functional areas, including optical, photonic, electrical, construction, thermal, mechanical, and biomedical applications. As shown in Fig. 9(b), a sub-micron-level woodpile-type 3D-printed TiO_2 mesh is produced for optical-phonic sensors with high refractive index and transparency.[108,109] As shown in Fig. 9(c), TiO_2 surface treatment on 3D-printed objects improved the measurement of transparent surfaces using optical profilometry. Thus, the custom TiO_2 treatments offered better cost-effectiveness, potentially less waste, and customizability than commercial treatments, such as aerosol and microemulsions.[110] The anatase TiO_2 in the 3D-printed structures demonstrated persistent photoluminescent properties due to slow electron migration, which is helpful for next-generation phantom PL imaging, as shown in Fig. 9(d).[111] The 3D-printed optical Ganzfeld bowl, coated with TiO_2 and serving as an integrating-sphere prototype, reflected all wavelengths equally and exhibited a radiance uniformity of 90%, comparable to the most expensive specialist coating, $BaSO_4$.[112] Vyatskikh *et al.* constructed and demonstrated 3D-printed TiO_2 with dielectric photonic crystal properties.[108] A 3D-printed TiO_2 thin film, serving as an electrode for a dye-sensitized solar cell, achieved a low sheet resistance of 6.8×10^6 Ω square^{-1} at a thickness of 6.25 μm, yielding an energy conversion efficiency of approximately 4%.[26] The simulated 3D-printed gyroid electrodes exhibit a greater concentration of Li^+ ions within the printed structure than in the bulk, and experimental results also confirm that the 3D-printed TiO_2 electrode delivers higher discharge capacities than sodium-ion and lithium-ion batteries.[113] The TiO_2 3D-printed monolithic ceramic filter exhibits excellent dielectric properties and effective filtering at microwave frequencies.[114,115] In addition, the 3D-printed TiO_2 resin exhibited strong gamma-ray attenuation with a low TiO_2 rate, demonstrating strong electromagnetic shielding properties.[116] A 3D-printed film combining a litmus indicator with TiO_2 functionality served as a pH sensor, and the fabricated sensor demonstrated excellent stability and reversibility.[117] Other well-studied non-catalytic functionalities of 3D-printed TiO_2 structures have been discussed in the following sections.

4.1 Construction applications

Incorporating TiO_2 into 3D-printed construction or building materials can give long-term photocatalytic capabilities, resulting in self-cleaning surfaces and air filtration with lower maintenance costs. In addition, TiO_2 played a crucial role in enhancing the quality, stability, and service life of cement in 3D-printed cementitious structures.[92] In the construction sector, the overall benefits of incorporating TiO_2 into 3D-printed cement materials are presented in Fig. 9(e). Moreover, in the TiO_2-dispersed cementitious composite, the added TiO_2 content helped reduce build time and significantly increased the number of printing layers compared to pristine cementitious materials, as shown in Fig. 9(f).[118] TiO_2 also improves hydration, density, compression strength, and thickening properties, thereby reducing slumping and flow diameter in 3D-

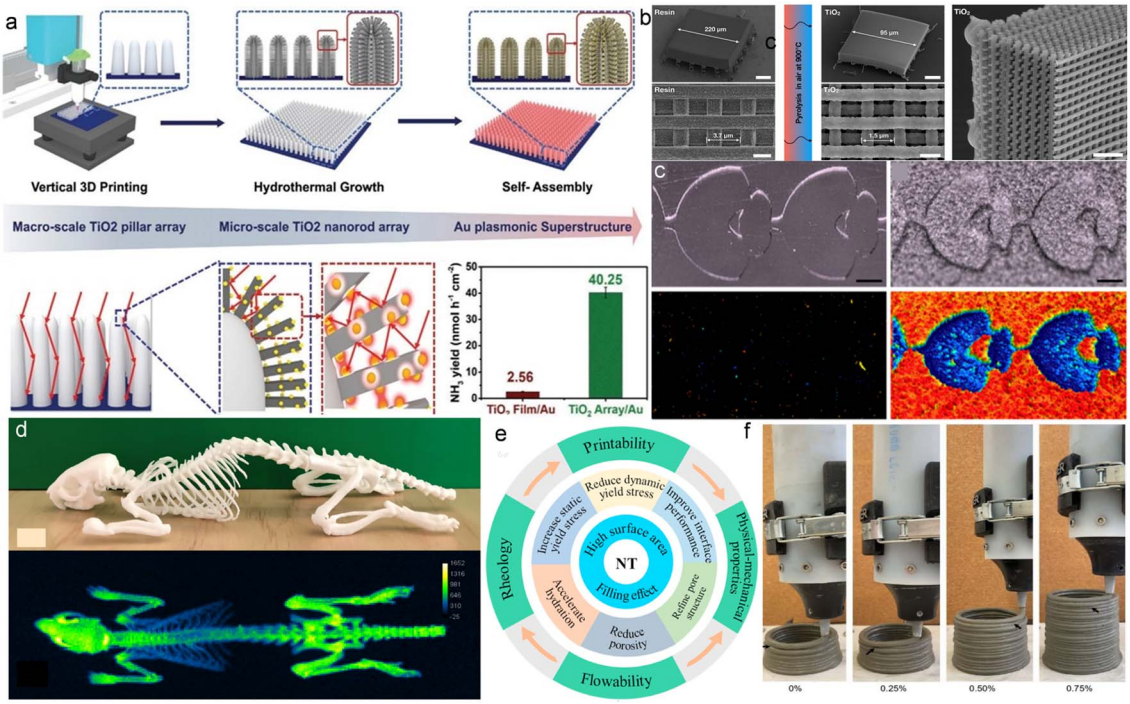

Fig. 9 (a) Schematic demonstration of the 3D-printing of forest-inspired hierarchical TiO_2/Au superstructure and related high light interaction-trapping mechanism and improved N_2 photo-fixation performance in 3D structure compared to a simple thin-film. Reproduced with permission from Wiley.[104] Copyright 2021. (b) Schematic of a dielectric photonic crystal, preceramic and calcinated 3D-printed TiO_2 woodpile architecture, and representative SEM images. Reproduced with permission from American Chemical Society.[108] Copyright 2020. (c) Optical profiling enhancement in the 3D-printed device by the incorporation of TiO_2.[110] (d) TiO_2 incorporated 3D-printed rat anatomical phantom and its improved PL imaging after light absorption.[111] (e) Various properties enhanced by the addition of nano TiO_2 in the 3D-printing cement. Reproduced with permission from Elsevier.[92] Copyright 2022. (f) Enhancement of printability (number of layers of 3D printing) of cement by increasing the TiO_2 concentration.[118]

printed cement, making it non-porous, stronger, and easier to build.[92] In addition, incorporating TiO_2 particles provided beneficial filling and nucleation effects in the cement-based material, specifically filling the voids within the 3D-printed specimens and increasing their density.[119] Moreover, the TiO_2 particles facilitated hydration by providing additional nucleation sites, thereby enhancing the compressive strength of the specimens under identical environmental conditions. The coating of TiO_2 onto the 3D-printed cement structure effectively degrades rhodamine B, opening the door to photocatalytic coatings in the construction industry for air filtration and self-cleaning.[75]

4.2 Thermal and mechanical applications

TiO_2 incorporated into a 3D-printed structural polymer enhances crystallinity, thermal stability (decomposition and glass transition temperatures), fluidity, and filament flowability, and manipulates surface texture (rough or smooth, depending on the matrix).[120–122] Further, the glass transition temperature of the 3D-printed polymers increased with increasing TiO_2 concentration.[123] The addition of TiO_2 to the 3D-printed Al_2O_3 led to increased ceramic grain growth and the formation of secondary Al_2TiO_5, thereby enhancing the bulk density, sintering kinetics, residual flexural strength, and thermal shock resistance.[124] Similarly, the addition of optimal MgO to the 3D-printed TiO_2 resulted in the growth of ceramic grains and the formation of secondary $MgTi_2O_5$, thereby enhancing the bulk density and bending strength and reducing the sintering temperature.[125] The mechanical stability and erosion resistance are also improved in the 3D-printed TiO_2 structures.[32] The tensile strength and elongation significantly improved with the addition of TiO_2 to the 3D-printed PLA structures.[122] As shown in Fig. 10(a), various mechanical properties, including tensile strength, modulus of elasticity, flexural strength, toughness, and microhardness, of the 3D-printed polymer structures improved upon incorporating TiO_2.[126,127] The addition of Zn to 3D-printed TiO_2 facilitated the formation of foam-like structures, yielding compression strengths and elastic moduli comparable to those of ceramic foams produced by conventional manufacturing techniques.[128] Overall, TiO_2-based 3D-printed composite structures enhance thermal and mechanical stability, making them suitable for load-bearing structural applications.

4.3 Biomedical applications

TiO_2 is also known as a bio-ceramic oxide with exceptional bioactivity and biocompatibility; hence, its 3D-printed structures are also being studied in the context of orthopedic scaffolds and dental fixations, where 3D printing methods enable the fulfillment of design complexity, arbitrary shaping, fast

production, and dimensional accuracy. The 3D-printed TiO_2 composite structures demonstrated improved bioactivity, enhanced cell proliferation and extracellular matrix mineralization, and facilitated osteogenic differentiation, offering optimal mechanical properties that support biomedical applications such as bone fixation and regenerative bone scaffolds.[22,130] As demonstrated in Fig. 10(b), the macro- and microporous 3D printed TiO_2 scaffold, which exhibits strong proliferation and osteogenic differentiation properties, further improves over time in rabbit bone marrow mesenchymal stem cells.[129] In comparison to 3D-Ti and TiO_2 scaffolds, the Ag-dispersed 3D-TiO_2 bone scaffolds showed significant amounts of uniformly distributed neo-plastic bone tissue in their pores, as well as genes and proteins associated with osteocalcin, collagen type I, and alkaline phosphatase that were more elevated and biocompatible with the surrounding tissues.[22] In addition, 3D-printed calcium silicate scaffold enriched with TiO_2 retains optimal porosity and demonstrates enhanced compressive strength, a slower degradation rate, and significantly increased osteogenic induction and angiogenic activity in bone regeneration. Furthermore, experiments using a cranial bone defect model have demonstrated that the 3D-printed calcium silicate/TiO_2 scaffold can significantly accelerate vascular neogenesis and bone regeneration, fully confirming its broad application potential in bone defect treatment.[131] The PLGA–TiO_2 composite scaffolds fabricated *via* 3D printing exhibited favorable mechanical and biological properties, supporting cell viability, osteoblast culture, enhanced calcium secretion, and increased ALP activity, all of which are essential for bone tissue regeneration.[132]

Both dental and bone-related structures require high mechanical strength, which is enhanced by increasing the TiO_2 concentration in the 3D-printed bio-parts.[88] Compositing PLA with TiO_2 significantly enhanced the mechanical, wear, and frictional properties of 3D-printed bio-components, which are highly desirable in regenerative bone-joint applications.[133] Other studies have revealed that 3D-printed TiO_2 composites exhibit good *in vitro* bioactivity and biocompatibility, including cell proliferation, viability, and adhesion, making them attractive candidates for biomedical applications in bone replacement treatments due to their cancellous bone-like characteristics and potential use in dental fixtures.[88,134,135] The exceptional mechanical strength, good antibacterial activity, and low cytotoxicity of the 3D-printed reinforced composite of PMMA/TiO_2/PEEK demonstrate tremendous promise as a material for realistic dental restorations.[136] Inspired by the organic-inorganic enamel biostructures of teeth, Wei *et al.* synthesized a TiO_2 columnar nanorod framework using microscale additive manufacturing.[137] The resultant design resembles an enamel-like structure, with comparable hardness, an ultra-high Young's modulus, and superior viscoelastic properties. The integration of TiO_2 nanoparticles into 3D-printed denture base resin significantly enhanced properties, including flexural strength/modulus, impact strength, Vickers hardness, DC, and solubility, compared to the unmodified material; however, the influence on saliva sorption and Martens hardness was negligible.[138] The addition of TiO_2 nanoparticles to 3D-printed dental resin restorations has strong potential to improve the longevity of long-term interim implant-supported restorations.[139] Furthermore, TiO_2-containing 3D-printed nanocomposite denture base resins exhibited increased surface roughness and color change without altering hardness; this impact was resin-dependent. Therefore, selecting an appropriate resin material for nanocomposite fabrication should be considered.[140]

Conclusively, the overall advantages of TiO_2 3D printing over traditional methods, including performance, are demonstrated in Table 3. As summarized in the table, 3D-printed TiO_2

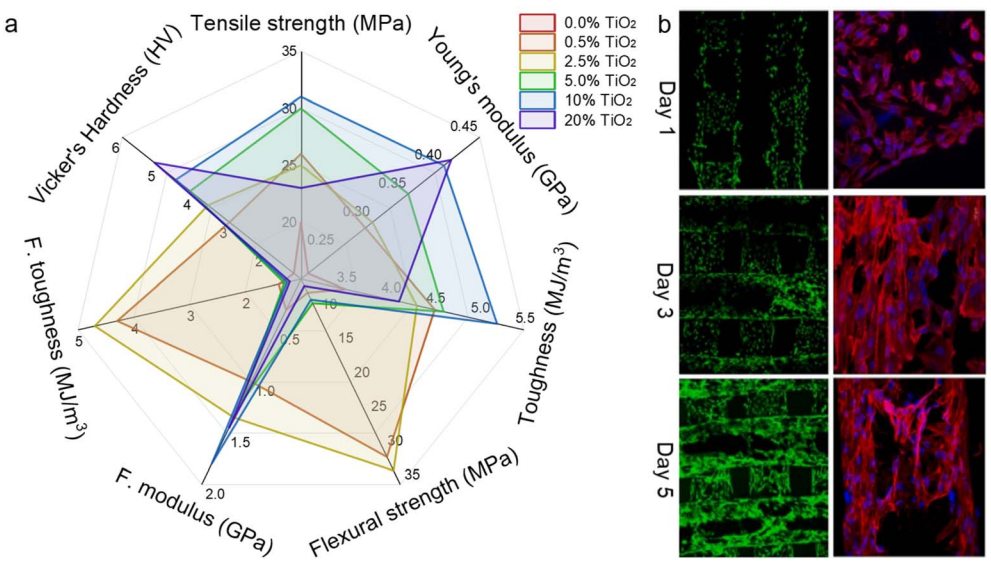

Fig. 10 (a) Various mechanical properties improved strongly by the incorporation of TiO_2.[126] (b) Live–dead and cytoskeleton-stained fluorescence images of cell proliferation on the TiO_2 3D-printed scaffolds with different pore sizes over time. Reproduced with permission from Elsevier.[129] Copyright 2024.

consistently outperforms powder dispersion and films across several key metrics, including light penetration, pollutant degradation kinetics, hydrogen productivity, structural integrity, and recovery and reusability.

5. Summary and future prospects

The integration of 3D printing technology with TiO_2 represents a significant breakthrough in photocatalysis and various multifunctional applications. This technology offers several unique advantages, including the ability to fabricate complex and precise geometries with tunable and integrated material properties, along with easy recyclability and reusability, making it a promising option for environmental remediation and ecological applications. This review provides a comprehensive overview of TiO_2 3D printing research and fabrication methods, while highlighting its potential for future innovations in the rapidly expanding fields of environmental remediation and other advanced functional applications. The literature available on 3D-printed TiO_2 architectures projects its suitability for clear real-world promise in the photocatalytic applications for a wide range of applications that include wastewater treatment, air purification, antimicrobial and self-cleaning surfaces, and hydrogen production. These applications are feasible mainly because in 3D printing, the catalyst can be immobilized within robust lattices and enable engineered flow and light management under practical operating conditions. 3D-printed TiO_2 architectures also show promise for other catalytic and non-catalytic applications, such as N_2 fixation, construction, thermal, mechanical, biomedical, and others. The 3D-printed TiO_2 architectures provide mechanical and thermal functionalities, such as improved tensile strength, flexural resilience, and higher glass-transition temperatures, and help in preserving a dual role: as a photocatalytic active surface and a stabilized structural component.

Regarding advancements in photocatalysis, future research should focus on the development of novel composite photocatalytic materials based on TiO_2 and the optimization of relevant 3D printing procedures to enhance the performance, stability, and durability, leading toward practical and large-scale applications. Furthermore, fabricating hybrid photocatalytic composite systems based on 3D-printed TiO_2, is expected to enhance photocatalytic efficiency. Research in this direction is demanding. Economically, these systems benefit from low-cost feedstocks and scalable additive manufacturing techniques such as DLP, DIW, and FDM. However, they still encounter significant challenges related to the cost of photopolymer resins, post-processing heat treatments, and relatively slow printing speeds, which currently limit their implementation to pilot-scale rather than fully commercial deployment. Long-term durability is considerably superior for 3D printing technology than that of powder- and film-based systems, as 3D-printed structures exhibit strong resistance to delamination, retain photocatalytic activity over repeated cycles, and effectively minimize nanoparticle leaching. It is envisioned that future studies should highlight, addressing the fouling and

Table 3 Advantages of 3D-printing over conventional power and film-based TiO_2

Performance metrics	Conventional TiO_2	Advantages of 3D-printed TiO_2	Evidence source
Light penetration efficiency	Minimal penetration in powders due to aggregation and dispersion issues[141]	Strong light-penetration enhancement. Customizable reactor geometry design	Fig. 5(a) demonstrates geometric enhancement through aligned and shifted woodpile architectures *versus* bulk materials
Photocatalytic degradation rate	Moderate rate with powder accumulations, gravity settling, and low-surface area exposure	Rapid kinetics expressed with multiple design optimizations	Table 1: DIW/woodpile structures degrade methylene blue (100% in 1.25 h) and triclosan (99.5% in 4 h) *versus* powder benchmarks requiring extended timeframes
Hydrogen generation capacity	Significantly lower volumetric H_2 output; rapid deactivation[95]	Higher production than TiO_2 powder; sustained performance over multiple cycles	Fig. 8(a): FCC lattice-structured aerogel demonstrates near-stoichiometric improvement; 3D architecture enables efficient light harvesting and gas-phase transport
Structural integrity, recovery, and recyclability	Either wash-out or cross-contamination from leaching particles[142]	Eliminates contamination risk; reusable across applications; self-supporting lattice structures with immobilization; zero nanoparticle leaching after multiple cycles	Conventional dip-coating and spraying methods produce non-uniform films prone to delamination, whereas 3D-printed monoliths achieve recovery without loss of catalytic activity
Mechanical & thermal robustness	Limited mechanical contribution in conventionally processed TiO_2	Dual functionality: photocatalytic + load-bearing capacity; enhanced tensile strength, modulus, and flexural resilience; improved glass transition temperature with loading	Incorporation into 3D polymer matrices elevates tensile strength by measurable margins and enables thermal stability up to controlled glass-transition temperatures, expanding applications in structural components

stability gaps *via* smarter geometries, doped composites, and surface modifications is essential to translating 3D-printed TiO_2 into reliable infrastructure technologies. Despite promising progress in 3D-printed TiO_2 structures, substantial future research is still required to address practicality parameters, such as scalability, techno-economic feasibility, long-term durability, operational stability, and commercialization prospects.

Author contributions

V. C. S. Theja and V. Karthikeyan: writing – original draft; Y. Guo and C. S. Yeung: literature review and data curation; S. Choudhary, V. Kannan, and D. S. Assi: writing review & editing; G. Saianand and G. A. Iyengar: conceptualization, editing, and funding; D.-E. Lee: funding acquisition; V. A. L. Roy: supervision, project administration, funding acquisition.

Conflicts of interest

The authors declare that they have no known competing financial interests or personal relationships that could have appeared to influence the work reported in this paper.

Data availability

Data sharing is not applicable to this article as no new data were generated or analyzed in this study.

Acknowledgements

This research was funded by the following grants: the Research Grants Council of the Hong Kong Special Administrative Region under the Institutional Development Scheme – Collaborative Research Grant Project (UGC/IDS(C)16/P01/24) and National Research Foundation of Korea grant funded by the Korean government (SMIT) (NRF-2022R1A2C1092289 and NRF-2018R1A5A1025137).

References

1 A. Meng, L. Zhang, B. Cheng and J. Yu, *Adv. Mater.*, 2019, **31**, 1807660.
2 Q. Guo, C. Zhou, Z. Ma and X. Yang, *Adv. Mater.*, 2019, **31**, 1901997.
3 S. Song, H. Song, L. Li, S. Wang, W. Chu, K. Peng, X. Meng, Q. Wang, B. Deng, Q. Liu, Z. Wang, Y. Weng, H. Hu, H. Lin, T. Kako and J. Ye, *Nat. Catal.*, 2021, **4**, 1032–1042.
4 B. Liu, Z. Hu, Y. Li, X. Tan, J. Ye and T. Yu, *Nat. Commun.*, 2025, **16**, 6014.
5 R. Wang, M. Shi, F. Xu, Y. Qiu, P. Zhang, K. Shen, Q. Zhao, J. Yu and Y. Zhang, *Nat. Commun.*, 2020, **11**, 4465.
6 A. Lamberti, M. Laurenti, D. Manfredi, C. Ricciardi and S. Stassi, *Adv. Mater. Technol.*, 2025, **10**, 2401142.
7 N. Munar Barceló, Y. Chen and K. Villa, *Adv. Sustainable Syst.*, 2025, **9**, e00748.
8 Q. Wei, H. Li, G. Liu, Y. He, Y. Wang, Y. E. Tan, D. Wang, X. Peng, G. Yang and N. Tsubaki, *Nat. Commun.*, 2020, **11**, 4098.
9 A. L. Barbosa, R. C. de Oliveira Romano, A. A. Bernardes and D. Gouvêa, *Ceram. Int.*, 2025, **51**, 24072–24079.
10 I. S. O. Barbosa, Y. A. Manrique, D. Paiva, J. L. Faria, R. J. Santos and C. G. Silva, *RSC Adv.*, 2025, **15**, 2275–2286.
11 C. Xu, T. Liu, W. Guo, Y. Sun, C. Liang, K. Cao, T. Guan, Z. Liang and L. Jiang, *Adv. Eng. Mater.*, 2020, **22**, 1901088.
12 B. Kaur, P. Singh, S. Thakur, A. Singh, V. Chaudhary, N. Kumar, A. A. P. Khan, M. A. Rub, N. Azum and P. Raizada, *J. Environ. Chem. Eng.*, 2025, **13**, 116042.
13 P. A. Gonzalez-Ocegueda, A. Herrera-Saucedo, J. G. Quiñones-Galvan, C. Valero-Luna, L. Alvarado-Perea, L. Canizales-Davalos, G. Martinez-Guajardo and A. Bañuelos-Frias, *Mater. Lett.*, 2021, **296**, 129873.
14 H. Sopha, A. Kashimbetova, L. Hromadko, I. Saldan, L. Celko, E. B. Montufar and J. M. Macak, *Nano Lett.*, 2021, **21**, 8701–8706.
15 H. Sopha, A. Kashimbetova, M. Baudys, P. K. Chennam, M. Sepúlveda, J. Rusek, E. Kolibalova, L. Celko, E. B. Montufar, J. Krysa and J. M. Macak, *Nano Lett.*, 2023, **23**, 6406–6413.
16 N. Saengchai, N. Hemha and W. Nuansing, *J. Phys.: Conf. Ser.*, 2023, **2653**, 012014.
17 Z. Zhan, W. Wu, J. Ye, L. Cui, Q. Yu, C. Chen and H. Qian, *Polym. Compos.*, 2025, **46**, 13032–13051.
18 M. Afshari, S. Bakhshi, M. R. Samadi and H. Afshari, *Polym. Eng. Sci.*, 2023, **63**, 267–280.
19 L. Ming, H. Yang, W. Zhang, X. Zeng, D. Xiong, Z. Xu, H. Wang, W. Chen, X. Xu, M. Wang, J. Duan, Y. B. Cheng, J. Zhang, Q. Bao, Z. Wei and S. Yang, *J. Mater. Chem. A*, 2014, **2**, 4566–4573.
20 J. A. Benavides-Guerrero, L. F. Gerlein, C. Trudeau, D. Banerjee, X. Guo and S. G. Cloutier, *Sci. Rep.*, 2022, **12**, 15441.
21 C. Y. Lee, A. C. Taylor, S. Beirne and G. G. Wallace, *Adv. Energy Mater.*, 2017, **7**, 1701060.
22 T. Liu, G. Yang, T. Li, Q. Wang, H. Liu and F. He, *Orthop. Surg.*, 2024, **16**, 1445–1460.
23 Z. Ji, Y. Wan, Y. Zou and H. Wang, *J. Alloys Compd.*, 2025, **1021**, 179620.
24 L. C. Caballero, J. S. Brindle, N. P. Ramey, S. A. Sufyan, S. K. Mohanty and M. M. Nigra, *J. Mater. Chem. A*, 2024, **12**, 20975–20989.
25 M.-K. Wang, F. Xiao and X. Xu, *Int. J. Implant Dent.*, 2025, **11**, 3.
26 A. Hansuebsai, K. Chareonsopa and K. Manseki, *Int. J. Thin Film Sci. Technol.*, 2020, **9**, 163–169.
27 K. Charoensopa, A. Hansuebsai and K. Manseki, *Key Eng. Mater.*, 2020, **843**, 79–83.
28 H. H. Do, T. K. C. Tran, T. D. T. Ung, N. T. Dao, D. D. Nguyen, T. H. Trinh, T. D. Hoang, T. L. Le and T. T. H. Tran, *J. Water Process Eng.*, 2021, **43**, 102319.
29 H. Chen, J. Wang, S. Peng, D. Liu, W. Yan, X. Shang, B. Zhang, Y. Yao, Y. Hui and N. Zhou, *Nano-Micro Lett.*, 2023, **15**, 180.

30 J. Guo, Y. Zeng, P. Li and J. Chen, *Ceram. Int.*, 2019, **45**, 23007–23012.
31 M. Rebber, M. Trommler, I. Lokteva, S. Ehteram, A. Schropp, S. König, M. Fröba and D. Koziej, *Adv. Funct. Mater.*, 2022, **32**, 2112914.
32 F. Mendez-Arriaga, M. Rodriguez-Hernandez and R. Almanza, *Mater. Sci. Semicond. Process.*, 2023, **167**, 107764.
33 M. Á. Gracia-Pinilla, N. A. Ramos-Delgado, C. Rosero-Arias, R. Sanders, S. Bartling, J. Winczewski, H. Gardeniers and A. Susarrey-Arce, *RSC Sustainability*, 2024, **2**, 3897–3908.
34 A. Vyatskikh, A. Kudo, S. Delalande and J. R. Greer, *Mater. Today Commun.*, 2018, **15**, 288–293.
35 C. H. Chen, S. C. Wang, H. W. Chen, T. Y. Chou and C. S. Chang, *ACS ES&T Water*, 2024, **4**, 1883–1893.
36 R. Zhou, R. Han, M. Bingham, C. O'Rourke and A. Mills, *Photochem. Photobiol. Sci.*, 2022, **21**, 1585–1600.
37 D. H. Kim, S. H. Nam, G. Han, S. R. Park, G. H. Jeong, S. Kim, Y. T. Cho and N. X. Fang, *APL Mater.*, 2024, **12**, 021001.
38 Z. Warren, T. T. Guaraldo, I. Barisic, G. A. Zoumpouli, J. Wenk and D. Mattia, *J. Mater. Chem. A*, 2024, **12**, 10913–10922.
39 R. Bernasconi, U. Bellè, S. Brigatti and M. V. Diamanti, *Addit. Manuf.*, 2024, **79**, 103916.
40 W. Huang, H. Mei, P. Chang, L. Pan, L. Cheng and L. Zhang, *Addit. Manuf.*, 2022, **58**, 103059.
41 S. Güler, A. Yavaş, B. Özler and A. Ç. Kilinç, *Rapid Prototyp. J.*, 2024, **30**, 1011–1022.
42 D. Wang, T. Zhi, L. Liu, L. Yan, W. Yan, Y. Tang, B. He, L. Hu, C. Jing and G. Jiang, *Sci. Total Environ.*, 2022, **815**, 152754.
43 A. Bansiddhi, G. Panomsuwan, C. Hussakan, T. L. Htet, B. Kandasamy, K. Janbooranapinij, N. Choophun, R. Techapiesancharoenkij, H. R. Pant, W. L. Ang and O. Jongprateep, *Top. Catal.*, 2023, **66**, 1662–1673.
44 M. Asava-arunotai, T. L. Htet, A. Bansiddhi, A. Lertworasirikul, K. Surawathanawises, T. Muangnapoh, B. Kandasamy, P. Kidkhunthod, G. Panomsuwan and O. Jongprateep, *Materialia*, 2024, **36**, 102139.
45 C. Li, Y. Zhang, C. Qiu, B. Yuan, R. Zhang, W. Li and H. Jin, *Colloids Surf., A*, 2023, **671**, 131570.
46 M. Mahmoud, J. Kraxner, A. Mehta, H. Elsayed, D. Galusek and E. Bernardo, *J. Eur. Ceram. Soc.*, 2024, **44**, 5449–5459.
47 M. Mariani, F. Nanni, C. Mazzuca and M. Bragaglia, *Ceram. Int.*, 2025, **51**, 722–734.
48 I. Barisic, R. Brucculeri, L. Airoldi, Z. Warren, A. S. Martins, M. Coduri, F. Auricchio, U. T. Anselmi and D. Mattia, *Appl. Mater. Today*, 2024, **38**, 102172.
49 D. C. Alves, P. M. Martins, R. Pinto, P. Costa, B. Bazán, R. F. de Luis, D. M. Correia and S. Lanceros-Méndez, *Appl. Mater. Today*, 2025, **44**, 102728.
50 H. T. Dung, N. T. Chinh, L. T. Lu and T. Hoang, *Vietnam J. Chem.*, 2021, **59**, 319–325.
51 M. A. Ávila-López, T. E. Lara-Ceniceros, F. E. Longoria, A. A. Elguezabal, A. Martínez De La Cruz, M. A. Garza-Navarro and J. Bonilla-Cruz, *ACS Appl. Nano Mater.*, 2022, **5**, 11437–11446.
52 L. Li, J. Li, H. Luo, S. Li and J. Yang, *Polymers*, 2022, **14**, 5435.
53 F. Mendez-Arriaga, E. de la Calleja, L. Ruiz-Huerta, A. Caballero-Ruiz and R. Almanza, *Mater. Sci. Semicond. Process.*, 2019, **100**, 35–41.
54 M. A. Torres Arango, D. Kwakye-Ackah, S. Agarwal, R. K. Gupta and K. A. Sierros, *ACS Sustainable Chem. Eng.*, 2017, **5**, 10421–10429.
55 L. Bergamonti, C. Bergonzi, C. Graiff, P. P. Lottici, R. Bettini and L. Elviri, *Water Res.*, 2019, **163**, 114841.
56 T. Liu, Y. Sun, B. Jiang, W. Guo, W. Qin, Y. Xie, B. Zhao, L. Zhao, Z. Liang and L. Jiang, *ACS Appl. Mater. Interfaces*, 2020, **12**, 28100–28109.
57 C. Fu, D. Li, J. Zhang, W. Guo, H. Yang, B. Zhao, Z. Chen, X. Fu, Z. Liang and L. Jiang, *Chem. Res. Chin. Univ.*, 2023, **39**, 891–901.
58 X. Guo, C. Chen, H. Jiao, W. Wu, Y. Jin, Z. Liang and B. Jiang, *Ind. Crops Prod.*, 2025, **225**, 120513.
59 M. Sevastaki, M. P. Suchea and G. Kenanakis, *Nanomaterials*, 2020, **10**, 2144.
60 A. D. McQueen, M. L. Ballentine, L. R. May, C. H. Laber, A. Das, M. J. Bortner and A. J. Kennedy, *ACS ES&T Water*, 2021, **2**, 137–147.
61 A. J. Calomeni-Eck, A. J. Kennedy, A. D. McQueen, M. L. Ballentine, B. M. Fernando, L. R. May and N. L. Melby, *J. Environ. Manage.*, 2024, **371**, 123208.
62 X. Chen, C. Zhang, X. Chen and N. Li, *Molecules*, 2025, **30**, 3891.
63 W. Jo, B. J. Yoon, H. Lee and M. W. Moon, *3D Print. Addit. Manuf.*, 2017, **4**, 222–230.
64 M. J. Martín de Vidales, A. Nieto-Márquez, D. Morcuende, E. Atanes, F. Blaya, E. Soriano and F. Fernández-Martínez, *Catal. Today*, 2019, **328**, 157–163.
65 A. Sangiorgi, Z. Gonzalez, A. Ferrandez-Montero, J. Yus, A. J. Sanchez-Herencia, C. Galassi, A. Sanson and B. Ferrari, *J. Electrochem. Soc.*, 2019, **166**, H3239–H3248.
66 M. R. Skorski, J. M. Esenther, Z. Ahmed, A. E. Miller and M. R. Hartings, *Sci. Technol. Adv. Mater.*, 2016, **17**, 89–97.
67 L. Bergamonti, C. Graiff, C. Bergonzi, M. Potenza, C. Reverberi, M. C. Ossiprandi, P. P. Lottici, R. Bettini and L. Elviri, *Catalysts*, 2022, **12**, 580.
68 P. Ortega-Columbrans, A. Ferrandez-Montero, J. Yus, A. J. Sanchez-Herencia and B. Ferrari, *Catal. Today*, 2024, **426**, 114371.
69 K. Miklec, I. Grčić, L. Radetić, I. K. Cingesar and D. Vrsaljko, *Coatings*, 2023, **13**, 386.
70 A. J. Kennedy, A. D. McQueen, M. L. Ballentine, L. R. May, B. M. Fernando, A. Das, K. L. Klaus, C. B. Williams and M. J. Bortner, *Chem. Eng. J.*, 2023, **455**, 140866.
71 Z. R. Yang, P. C. Lee, C. Y. Kuo, C. H. Shin and C. Bin Lin, *Int. J. Adv. Manuf. Technol.*, 2022, **120**, 4539–4550.
72 Y. Wei, M. Chen, S. Guo, Y. Li, Z. Zhang, Y. Xie, C. Cai and Q. Wei, *ACS ES&T Water*, 2024, **4**, 1590–1600.

73 I. Syngelakis, M. Manousidaki, E. Kabouraki, A. Kyriakakis, G. Kenanakis, A. Klini, S. Tzortzakis and M. Farsari, *J. Appl. Phys.*, 2023, **134**, 233101.
74 M. Grandcolas and A. Lind, *Mater. Lett.*, 2022, **307**, 131044.
75 B. Zahabizadeh, I. Rocha Segundo, J. Pereira, E. Freitas, A. Camões, V. Teixeira, M. F. M. Costa, V. M. C. F. Cunha and J. O. Carneiro, *J. Build. Eng.*, 2023, **70**, 106373.
76 M. Grandcolas, A. Lind and C. Grande, *Mater. Res. Bull.*, 2025, **188**, 113407.
77 G. C. Tedesco, C. A. Joll, W. P. Ela, A. Pivrikas and D. J. Henry, *ChemistrySelect*, 2023, **8**, e202300288.
78 U. Malik, M. Mazur, D. D. Mandaliya, R. D. Gudi, S. Periasamy and S. K. Bhargava, *ACS Omega*, 2025, **10**, 13453–13464.
79 R. Bernasconi, E. Carrara, M. Hoop, F. Mushtaq, X. Chen, B. J. Nelson, S. Pané, C. Credi, M. Levi and L. Magagnin, *Addit. Manuf.*, 2019, **28**, 127–135.
80 G. V. Theodorakopoulos, M. K. Arfanis, T. Stepišnik Perdih, S. Malamis, D. Iatrou, G. E. Romanos and P. Falaras, *Environments*, 2024, **11**, 156.
81 V. Ciobanu, T. Galatonova, T. Braniste, P. Urbanek, S. Lehmann, B. Hanulikova, K. Nielsch, I. Kuritka, V. Sedlarik and I. Tiginyanu, *Sci. Rep.*, 2024, **14**, 31215.
82 Y. Majooni, S. P. Sava, K. Fayazbakhsh and N. Yousefi, *Adv. Sustainable Syst.*, 2025, **9**, e00135.
83 Y. Ji, Z. Su, X. Cui, Z. Geng and C. Wang, *Desalination*, 2025, **610**, 118914.
84 L. Han, L. Shen, H. Lin, Z. Huang, Y. Xu, R. Li, B. Li, C. Chen, W. Yu and J. Teng, *Chemosphere*, 2023, **315**, 137791.
85 A. López-Camacho, M. J. Grande, D. Carazo-Álvarez and M. D. La Rubia, *J. Vinyl Addit. Technol.*, 2025, **31**, 1151–1171.
86 N. Vidakis, M. Petousis, N. Mountakis, E. Maravelakis, S. Zaoutsos and J. D. Kechagias, *Int. J. Adv. Manuf. Technol.*, 2022, **121**, 785–803.
87 G. Remaggi, L. Bergamonti, C. Graiff, M. C. Ossiprandi and L. Elviri, *Antibiotics*, 2023, **12**, 1104.
88 B. Aktas, R. Das, A. Acikgoz, G. Demircan, S. Yalcin, H. G. Aktas and M. V. Balak, *Mater. Today Commun.*, 2024, **38**, 107872.
89 Z. Mai, D. Liu, Z. Chen, D. Lin, W. Zheng, X. Dong, Q. Gao and W. Zhou, *Polymers*, 2021, **13**, 2196.
90 J. Luo, G. Xia, L. Liu, A. Ji and Q. Luo, *Foods*, 2022, **11**, 3286.
91 A. López-Camacho, M. J. Grande, D. Carazo-Álvarez and M. D. La Rubia, *Mater. Lett.*, 2024, **372**, 137039.
92 Q. Liu, Q. Jiang, M. Huang, J. Xin and P. Chen, *J. Cleaner Prod.*, 2022, **379**, 134804.
93 M. Z. Hussain, P. F. Großmann, F. Kohler, T. Kratky, L. Kronthaler, B. van der Linden, K. Rodewald, B. Rieger, R. A. Fischer and Y. Xia, *Sol. RRL*, 2022, **6**, 2200552.
94 M. Kubovics, C. G. Silva, A. M. López-Periago, J. L. Faria and C. Domingo, *Gels*, 2022, **8**, 719.
95 M. Rebber, H. Sannemüller, M. Jaruszewski, D. Pfannkuche, A. Urakawa and D. Koziej, *Chem. Mater.*, 2023, **35**, 3849–3858.
96 M. Schreck, N. Kleger, F. Matter, J. Kwon, E. Tervoort, K. Masania, A. R. Studart and M. Niederberger, *Small*, 2021, **17**, 2104089.
97 A. Castedo, E. Mendoza, I. Angurell and J. Llorca, *Catal. Today*, 2016, **273**, 106–111.
98 H. Song, G. Ran, J. Xu, C. Lin, Z. Yang, Y. Chang, W. Zhou, H. Li, X. Wang and J. Wang, *J. Alloys Compd.*, 2025, **1016**, 178941.
99 A. Elkoro, L. Soler, J. Llorca and I. Casanova, *Appl. Mater. Today*, 2019, **16**, 265–272.
100 L. Chen, X. Tang, P. Xie, J. Xu, Z. Chen, Z. Cai, P. He, H. Zhou, D. Zhang and T. Fan, *Chem. Mater.*, 2018, **30**, 799–806.
101 H. Oh, H. Charles, T. Im, H. Khan and C. S. Lee, *Int. J. Adv. Manuf. Technol.*, 2024, **130**, 2731–2742.
102 R. Han, R. Zhou, C. O'Rourke and A. Mills, *J. Photochem. Photobiol., A*, 2023, **443**, 114843.
103 G. F. Binetti Basterrechea, V. N. Montesinos and N. Quici, *Heliyon*, 2023, **9**, e22635.
104 W. Guo, Y. Liu, Y. Sun, Y. Wang, W. Qin, B. Zhao, Z. Liang and L. Jiang, *Adv. Funct. Mater.*, 2021, **31**, 2100768.
105 Z. Wang, J. Du, X. Zhang, Z. Guo, Z. Zhang and W. Wen, *Microchim. Acta*, 2025, **192**, 162.
106 C. Zhang, Y. Zhang, Y. Wang, J. Liu, Y. Chang, T. Qin, Y. Cao, X. Bao, P. Li, Z. Yang and Y. Zhang, *Biosens. Bioelectron.*, 2025, **276**, 117271.
107 Z. Xue, X. Liang, J. Li, M. Yu, Y. Ru, Q. Li and H. Sun, *J. Electrochem. Soc.*, 2025, **172**, 050505.
108 A. Vyatskikh, R. C. Ng, B. Edwards, R. M. Briggs and J. R. Greer, *Nano Lett.*, 2020, **20**, 3513–3520.
109 A. Vyatskikh, R. C. Ng, B. Edwards and J. R. Greer, *Proc. SPIE*, 2019, **10930**, 22–28.
110 I. Semmes, G. K. Lorio, F. V. Kewir, J. A. Belgodere and W. T. Monroe, *ACS Appl. Opt. Mater.*, 2025, **3**, 871–880.
111 T. Dann, J. Raphel, S. T. Gammon, Z. Mastrovich, T. Van Avermaete, J. Jeffrey, S. Adusumilli and W. M. Leevy, *Materials*, 2021, **14**, 1813.
112 J. Gale, S. Sartie, P. Dougherty, C. Allen, M. Bagley, M. Münch and S. Fraser, *Med. Eng. Phys.*, 2025, **142**, 104372.
113 A. Maurel, A. C. Martinez, S. B. Chavari, B. Yelamanchi, M.-L. Seol, D. A. Dornbusch, W. H. Huddleston, S. T. Sreenivasan, C. G. Sherrard, E. MacDonald and P. Cortes, *J. Electrochem. Soc.*, 2023, **170**, 100538.
114 Q. Liu, M. Qiu, L. Shen, C. Jiao, Y. Ye, D. Xie, C. Wang, M. Xiao and J. Zhao, *Electronics*, 2019, **8**, 1067.
115 M. Akhmatnabiev, A. Petrov, M. Timoshenko, M. Sychov, S. Diachenko, M. Arsentev, A. Bakulin, E. Skorb and M. Nosonovsky, *Biomimetics*, 2025, **10**, 804.
116 Y. Kavun, N. Çelikçi and S. Kerli, *Appl. Radiat. Isot.*, 2026, **208**, 112368.
117 M. P. Marković, E. Forjan, P. Kassal, A. Nosić and D. Vrsaljko, *Appl. Sci.*, 2025, **15**, 2488.
118 P. de Matos, T. Zat, K. Corazza, E. Fensterseifer, R. Sakata, G. Mohamad and E. Rodríguez, *Materials*, 2022, **15**, 3896.
119 J. Liu, P. Li, D. Jin, S. Her, J. Kim, Y. Yoon, M. Baldassari and S. Bae, *J. Build. Eng.*, 2023, **72**, 106618.

120 M. Yilmaz, *J. Thermoplast. Compos. Mater.*, 2026, **39**, 172–197.
121 S. Bergaliyeva, D. L. Sales, J. M. Jiménez Cabello, P. Burgos Pintos, N. Fernández Delgado, P. Marzo Gago, A. Zammit and S. I. Molina, *Polymers*, 2023, **15**, 3458.
122 S. Patel, G. S. Sudha, N. R. Aswathy, A. K. Mohapatra and P. C. Padhi, *J. Mater. Eng. Perform.*, 2026, **35**, 344–354.
123 Y. Liu, J. Chen, L. Ning, J. Sun, L. Liu and K. Zhao, *e-Polymers*, 2022, **22**, 686–695.
124 Y. Qiu, Q. Li, J. Liang, B. Qu, X. Liang, S. Liu, Y. Zhou, X. Sun and J. Li, *Ceram. Int.*, 2025, **51**, 17453–17462.
125 B. Hu, W. Zou, W. Wu, J. Tang, R. Chen, H. Zhou, C. Du and B. Shan, *J. Eur. Ceram. Soc.*, 2022, **42**, 1694–1702.
126 N. Vidakis, M. Petousis, A. Maniadi, V. Papadakis and A. Manousaki, *J. Compos. Sci.*, 2022, **6**, 209.
127 N. Vidakis, M. Petousis, A. Maniadi, E. Koudoumas, M. Liebscher and L. Tzounis, *Polymers*, 2020, **12**, 1589.
128 A. H. Aleni, N. Kretzschmar, A. Jansson, I. F. Ituarte and L. St-Pierre, *Ceram. Int.*, 2020, **46**, 16725–16732.
129 S. Wang, S. Zhang, Y. Cui, X. Lu, M. Zhang, J. Chen, Y. Cao, C. Zhou and B. Yang, *Ceram. Int.*, 2024, **50**, 20410–20420.
130 M. Yilmaz and D. Kapusuz Yavuz, *Bioprinting*, 2025, **49**, e00420.
131 Z. Huang, X. Wang, Z. Zhang, B. Yu, S. Wang, X. Chen, Y. Zhang, J. Yang, Z. Zeng and Z. Dong, *Mater. Des.*, 2025, **255**, 114166.
132 M. Rasoulianboroujeni, F. Fahimipour, P. Shah, K. Khoshroo, M. Tahriri, H. Eslami, A. Yadegari, E. Dashtimoghadam and L. Tayebi, *Mater. Sci. Eng., C*, 2019, **96**, 105–113.
133 M. Olam and N. Tosun, *Polym. Adv. Technol.*, 2025, **36**, e70175.
134 S. E. Nájera, M. Michel and N. S. Kim, *MRS Adv.*, 2018, **3**, 2373–2378.
135 B. Bulut and Ş. Duman, *Ceram. Int.*, 2022, **48**, 21378–21388.
136 S. G. Chen, J. Yang, Y. G. Jia, B. Lu and L. Ren, *Nanomaterials*, 2019, **9**, 1049.
137 J. Wei, H. Ping, J. Xie, Z. Zou, K. Wang, H. Xie, W. Wang, L. Lei and Z. Fu, *Adv. Funct. Mater.*, 2020, **30**, 1904880.
138 A. Altarazi, J. Haider, A. Alhotan, N. Silikas and H. Devlin, *Dent. Mater.*, 2023, **39**, 1122–1136.
139 N. S. ElMalah, Y. Ibrahim and D. Mostafa, *BMC Oral Health*, 2025, **25**, 806.
140 M. A. AlGhamdi, S. M. Fouda, Y. A. Al-Dulaijan, S. Q. Khan, M. El Zayat, R. Al Munif, Z. Albazroun, F. H. Amer, A. T. Al Ammary, A. A. Mahrous and M. M. Gad, *Front. Dent. Med.*, 2025, **6**, 1581461.
141 H. Khan and M. U. H. Shah, *J. Environ. Chem. Eng.*, 2023, **11**, 111532.
142 O. Cabezuelo, L. N. Ponce-Gonzalez, M. L. Marin and F. Bosca, *Appl. Mater. Today*, 2023, **35**, 101947.